

# Multi-scale physics of cryogenic liquid helium-4: Inverse coarse-graining properties of smoothed particle hydrodynamics

Satori Tsuzuki (都築 怜理)<sup>a</sup>

<sup>a</sup>Research Center for Advanced Science and Technology, The University of Tokyo, 4-6-1, Komaba, Meguro-ku, Tokyo 153-8904, Japan

---

## Abstract

Recent numerical studies on cryogenic liquid helium-4 have provided a multiscale physics perspective based on Landau's two-fluid model. This study presents the possibility that two-fluid models based on classical and quantum hydrodynamics have a relationship between scale transformation by filtering in large eddy simulations (LES) and inverse scale transformation using smoothed particle hydrodynamics (SPH). We consider that the spin angle momentum conservation term, which we previously introduced into the two-fluid model as a quantum mechanical correction, formally corresponds to the subgrid-scale (SGS) model, which can be derived from the scale transformation of the two-fluid model from quantum to classical hydrodynamics. We demonstrate that solving the two-fluid model based on classical hydrodynamics using SPH can reproduce the fluctuations at the microscopic scale because the truncation errors owing to the smoothing kernel approximation can substitute the fluctuations at the microscopic scale. In particular, the fluctuations can be reproduced at more macroscopic scales and amplified according to the size of kernel radius. Our results and discussion provide new insights into the microscopic composition of cryogenic liquid helium-4 within a multiscale framework. First, a normal fluid can be a mixture of inviscid and viscous particles. Second, a flow identified as a normal fluid on the microscopic scale because of the presence of molecular viscosity is still classified as an inviscid fluid on the hydrodynamic scale because its viscosity is insufficient to produce eddy viscosity. In conclusion, we provide a new multiscale physical framework for cryogenic liquid helium-4.

*Keywords:* Multi-scale physics, quantum hydrodynamics, cryogenic liquid helium-4, smoothed particle hydrodynamics, inverse coarse-graining effects, large eddy simulation

---

## 1. Introduction

The peculiar behavior of liquid helium-4, caused by its loss of viscosity at cryogenic temperatures near absolute zero, has long captivated scientists. An atom of liquid helium-4 consists of four nucleons, two neutrons and two protons, and thus has the property of having an integer multiple of angular momentum, known as “bosons”. Liquid helium-4 in the bulk state is a quantum many-body interacting system for bosons. The essential mechanism of liquid helium-4 has been extensively studied, particularly in the field of condensed matter physics. Historically, the research began with the successful liquefaction of helium-4 by H. K. Onnes [1, 2], followed by the discovery of the superfluidity of liquid helium by P. L. Kapitza [3] and the explanation of superfluidity based on the Bose–Einstein Condensate (BEC) theory by F. W. London [4]. By the middle of the 20th century, the essential properties were roughly understood. Notably, many particles are in the ground state below the critical temperature (approximately 2.17 K at a given pressure), and the kinetic energy of the respective particles is limited to the zero-point vibrational energy on the scale of the reduced Planck's constant. This is an extremely small energy state that can be neglected in the classical mechanical regime. Moreover, because helium-4 is a monatomic molecule belonging to the noble-gas family, its electron orbitals are in a stable configuration, polarizations rarely occur, and van der Waals forces between the atoms are hardly exerted. Accordingly, the atomic interactions for attraction and repulsion are rare, and the molecular and hydrodynamic viscosities are drastically reduced. In experiments, E.F. Burton reported a decrease in viscosity by a

---

*Email address:* tsuzukisatori@g.ecc.u-tokyo.ac.jp (Satori Tsuzuki (都築 怜理))

factor of eight before and after the lambda point at a high Reynolds number, and Kapitza reported a decrease by a factor of at least 1500 for a laminar flow [3, 5–8].

Concurrently, the phenomenological properties of liquid helium-4 were also studied. In particular, the two-fluid model proposed by L. Tisza [9] and L. Landau [10] adopted the concept of coexistence of two components at finite cryogenic temperature: a “superfluid” component with no viscosity and a “normal” fluid component with viscosity. In principle, the ratio of these components follows the quantum statistics of bosonic particles. Their original two-fluid model described the counterflow experiments well, especially when a small amount of heat (e.g.,  $50\mu W$ ) flowed into the system through an attached heater. Furthermore, the two-fluid model theoretically indicated the existence of sound waves in liquid helium-4 in terms of pressure and temperature, which was confirmed experimentally. Nevertheless, Landau’s two-fluid model could not explain the experimental results for the relationship between the inflow heat rate and velocity of the components when the inflow heat rate was high. However, in 1949, C. J. Gorter and J. H. Mellink theoretically and experimentally showed that mutual friction occurs between the two components, which were previously considered to exist independently, and successfully explained the counterflow of liquid helium phenomenologically on a broader scale [11]. In this paper, we refer to the Landau’s two-fluid model with the mutual friction terms proposed by Gorter and Mellink as the “two-fluid model based on quantum hydrodynamics.” Recently, counterflow was described from a microscopic perspective by considering the interactions between normal fluid components and quantum vortices, which emerge as the fluid velocity exceeds Feynman’s critical velocity [12], after which the perfect superfluid state begins to break. A quantum vortex is a vortex that is unique to quantum fluids and is not observed in classical fluid mechanics. In liquid helium-4 at cryogenic temperatures, vortices do not dissipate but exist in stable states because the circulation of each vortex is quantized owing to the quantization of the phase of the wave function. In general, the relationship between a quantum vortex and the velocity field generated by the vortex around it can be described by the Biot–Savart law, and the method of solving the Biot–Savart law directly or under a local approximation is known as the vortex filament model (VFM) [13–16]. Recent numerical studies on the counterflow of superfluid helium-4 have adopted the coupling method of the VFM with the Navier–Stokes (NS) equations [17–21]. The quantization of the circulation has a significant impact not only on shear flow-dominated problems, such as counterflow, but also on rotational phenomena. It is known that the quantization of the circulation leads to a phenomenon called “persistent current,” in which the superfluid continues to flow for a very long time in a toroidal vessel by reaching a steady state of flow velocity [22]. In particular, the measured angular momentum of the fluid differs from that of classical fluids. Furthermore, in the problem of horizontally rotating liquid helium-4, quantum vortex lattice phenomena are observed [23–30], i.e., quantum vortices are oriented in the same direction, are equally spaced in a lattice, and rigidly rotate around the rotation axis of the container at a speed proportional to the distance from the rotation axis. The torus flow and quantum vortex lattice phenomena illustrated herein are representative examples that characterize the unique nature of the rotational phenomena of liquid helium-4.

Thus, liquid helium-4 has been studied mainly from the viewpoint of quantum mechanics or quantum hydrodynamics, and most existing numerical models target nanometer-scale phenomena. Therefore, simulating the problems of bulk liquid helium-4 in the scale of centimeters to meters using existing methods inevitably involves the use of an enormous number of particles or spatial grids, which is impractical even with state-of-the-art supercomputers. We now consider the spatial scales of large-scale problems involving bulk liquid helium-4, such as film flow [31] (fluid spontaneously crawling out of a container due to viscous disappearance) and fountain phenomena [32], in which a container filled with a porous medium at its bottom and installed with an opening at its top is half immersed in a reservoir of superfluid liquid helium-4; as the upper part of the container is heated, the loss of viscosity allows the liquid helium to pass through the porous medium, and the fluid moves to resolve the concentration difference between the two components, resulting in a fluid jet from the top of the container. These phenomena are often referred to as “macroscopic quantum phenomena” because they exhibit bizarre phenomena due to the disappearance of molecular viscosity, although they are large-scale problems of centimeters to meters in size that can be observed with the naked eye in the classical hydrodynamic regime governed by the NS equations. The same holds true for the rotational problems. In vortex lattice phenomena, the vortex center size of a vortex in a quantum vortex lattice is on the angstrom scale, whereas the size of the velocity field created by the surrounding quantum vortex is on the order of micrometers, and the scale of the vortex lattice is on the order of micrometers to centimeters. To give an example, in the problem of horizontally rotating liquid helium-4 in a circular vessel with 1 cm in diameter, the theoretical vortex distance calculated from Feynman’s rule [33, 34] when the vessel is forced to rotate around its central axis at a speed of  $5 \text{ rad} \cdot \text{s}^{-1}$  is  $10^{-2} \text{ cm}$  for a circulation quantum  $\kappa \approx 10^{-3} \text{ cm}^2/\text{s}$ . Therefore, vortex lattice phenomena are sufficiently macroscopic

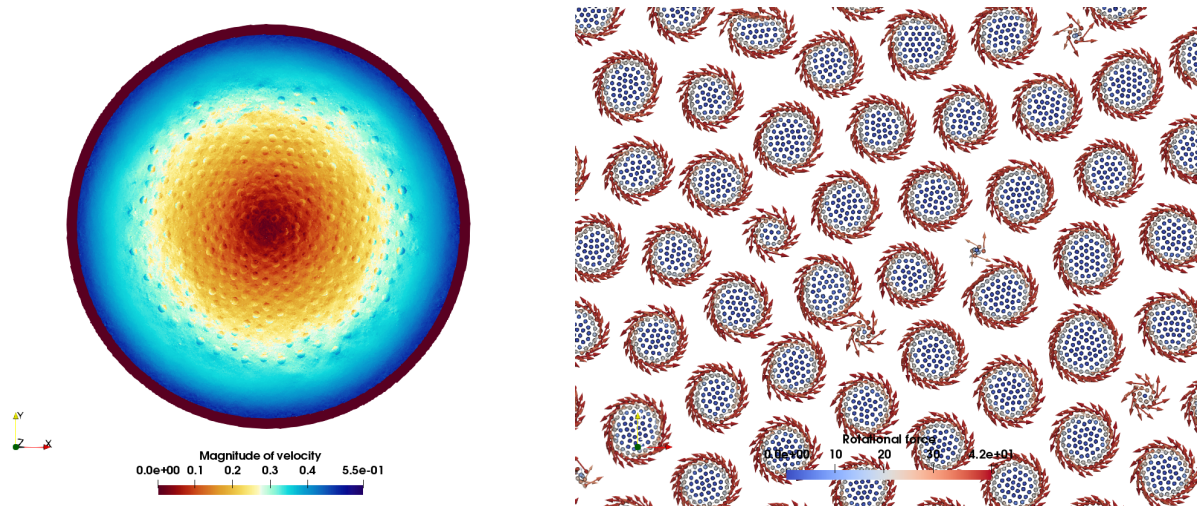


Figure 1: Snapshot of the replicated simulation reported in Refs. [28, 36] under the same conditions: (a) shows the intensity distribution of the particle velocity, and (b) is an enlarged view of (a), visualized by the direction and intensity of the rotational force of individual vortices as arrow vectors and color maps, respectively (Multimedia view).

fluid phenomena, and the lattice size belongs to the classical hydrodynamic regime. In addition, in an experiment on the persistence in a torus vessel, the diameter of the tube was approximately 5 mm and the length of the circumference of the tube was approximately 31.4 cm [22]. Therefore, macroscopic quantum phenomena belong to the classic hydrodynamic regime category. Currently, no simulation method has been established that can solve the NS equation while reproducing macroscopic quantum phenomena with high accuracy. In addition, the viscosity in rotational problems exhibits a complex behavior compared with that in problems in which shear viscosity is dominant. In the experiment using a rotational viscometer, the rotational viscosity of liquid helium-4 suddenly decreased when cooled to a critical temperature; however, it immediately increased again when cooled further below the critical temperature, and finally diverged near absolute zero [35]. In summary, there is still much room for investigation into the basic mechanism of the rotational phenomena, and no simulation method that can numerically reproduce the dynamics of bulk liquid helium with macroscopic quantum phenomena has been established.

To overcome this problem, the author studied a numerical simulation method that approaches the dynamics of liquid helium-4 in the bulk state from the viewpoint of fluid dynamics with the aim of numerically reproducing macroscopic quantum phenomena. We focused on the following facts reported in previous studies: Landau’s two-fluid model solved the Euler equation for an inviscid fluid and the NS equation for a viscous fluid independently; however, it was later recognized that mutual friction between the two components was activated when the inflow heat rate was large. Accordingly, the fact that the two components interact under certain conditions allows us to assume that a two-phase flow model consisting of viscous and inviscid fluids can approximate the dynamics of cryogenic liquid helium-4 provided that appropriate particle corrections are considered. We now distinguish between quantum and particle corrections. A quantum correction does not consider the zero limit of Planck’s constant  $h$ , that is, corrections that make physical quantities such as energy and angular momentum scalar multiples of  $h$  or add a correction term that includes  $h$ . In contrast, particle correction manifests properties as particles that break the continuum approximation. In our previous study, by utilizing the mathematical or formal similarity between the “two-fluid model based on quantum hydrodynamics” and the classical two-phase flow model, we discretized the set of equations for inviscid and viscous fluids by considering them as a classical two-phase system that admits the existence of a fluid force toward the other fluid component, while allowing particle correction at the interface and spin angular momentum conservation as a sort of quantum correction. Hereafter, our two-fluid model is referred to as the two-fluid model based on classical hydrodynamics, the proposed two-fluid model, or simply our two-fluid model.

In this previous work, we discretized the system of equations using smoothed particle hydrodynamics (SPH) [38–44], which is a Lagrangian numerical scheme, to conserve the variables for each constituent particle. The discretization of the system of equations for a classical fluid using SPH makes it possible to describe a fluid that is a continuum as a many-particle interacting system consisting of fluid particles. In mathematical terms, the discretization of this type is also referred to as the “finite particle approximation” of a continuum. In classical fluids, each fluid particle

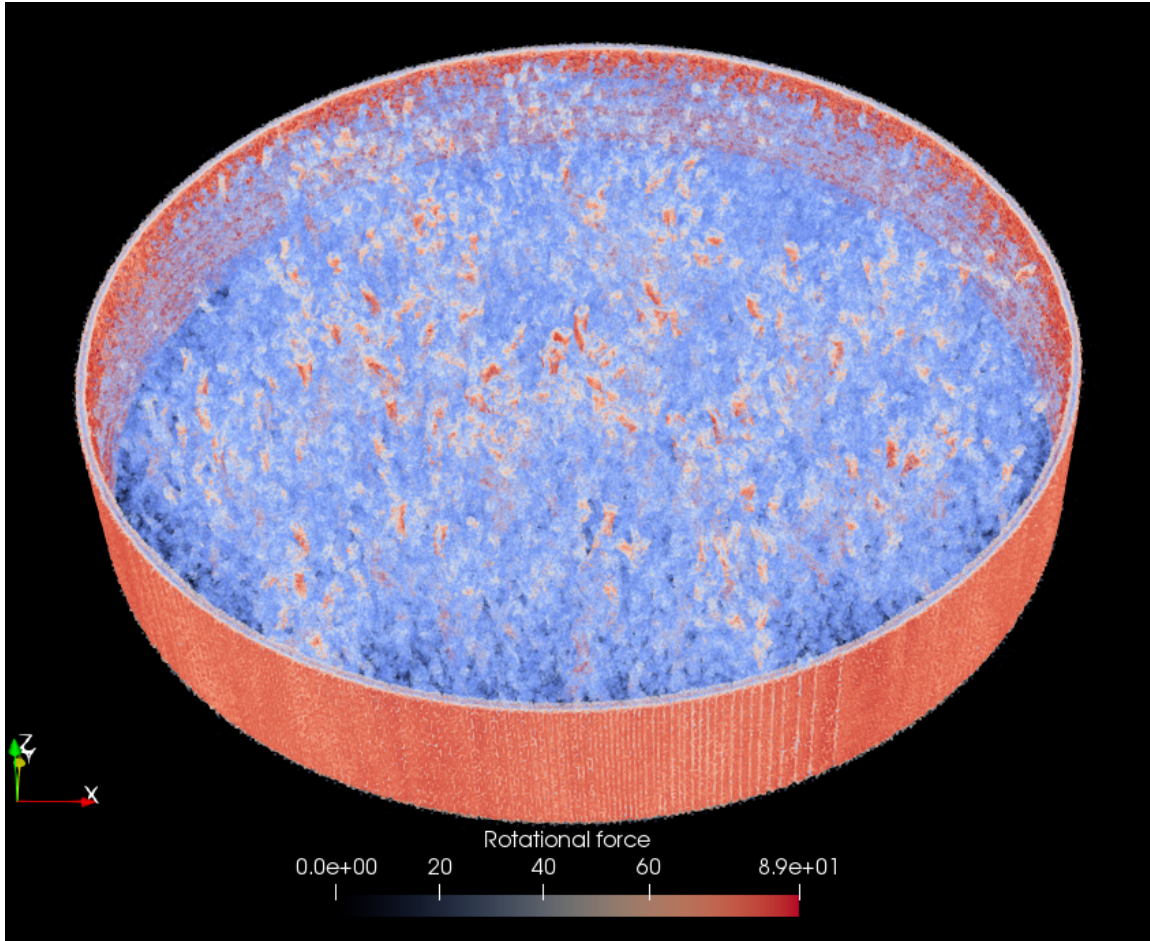


Figure 2: Snapshot of the replicated simulation reported in Ref. [37] under the same conditions; we can observe the liquid helium-4 rotating only in the horizontal direction with a certain thickness.

is only a fragment of a continuum; therefore, it has no physical significance. However, liquid helium-4 at cryogenic temperatures is essentially a multiparticle-interacting system of bosonic particles. Accordingly, if we focus on liquid helium-4 at cryogenic temperatures, individual virtual particles can be given an “ontological” meaning corresponding to Bose particles in quantum mechanics rather than as fragments of a continuum in phenomenological descriptions. In other words, fluid particles in classical fluid mechanics can be considered as representative points of atoms and molecules or coarse-grained particles. It may be appropriate to consider them only as classical virtual particles until a specific correspondence between the fluid and microscopic particles is clarified. Nevertheless, formal similarities exist between the finite-particle approximation system of the two-fluid model and the quantum many-body system, which can be utilized to conserve the rotational angular momentum around the axes of the constituent particles. In a quantum many-body system, each atomic particle has quantized spin angular momentum. In this regard, SPH can conserve the constant angular momentum around the respective particles, ensuring the locality of the rotational angular momentum conservation. Let us consider a two-dimensional (2D) case as an example. From a classical mechanical perspective, if the individual particles are vertically oriented, undeformed, and have uniform physical properties, they can be assumed to be rigid. In this case, if the angular velocity around the axis of a fluid particle is maintained constant, the spin angular momentum of the particle is conserved. The spinning of particles around the axes is only a classical mechanical picture and does not necessarily indicate the kinetics of a quantum mechanical microscopic particle. Nevertheless, the mathematical property of the quantized angular momentum can be reproduced regardless of the actual kinematic picture.

The spin angular momentum-conserving NS equation was originally derived for polar fluids in 1964 by Condiff et al. [45]. In 2015, K. Müller presented a discrete SPH model for the spin angular momentum, conserving the NS equation within the framework of smoothed dissipative particle dynamics (SDPD) [46], in a numerical study of suspension flow problems such as blood flow. Inspired by these studies, we applied similar techniques to the NS equation for the normal fluid component in Landau’s two-fluid model to realize the conservation of spin angular momentum

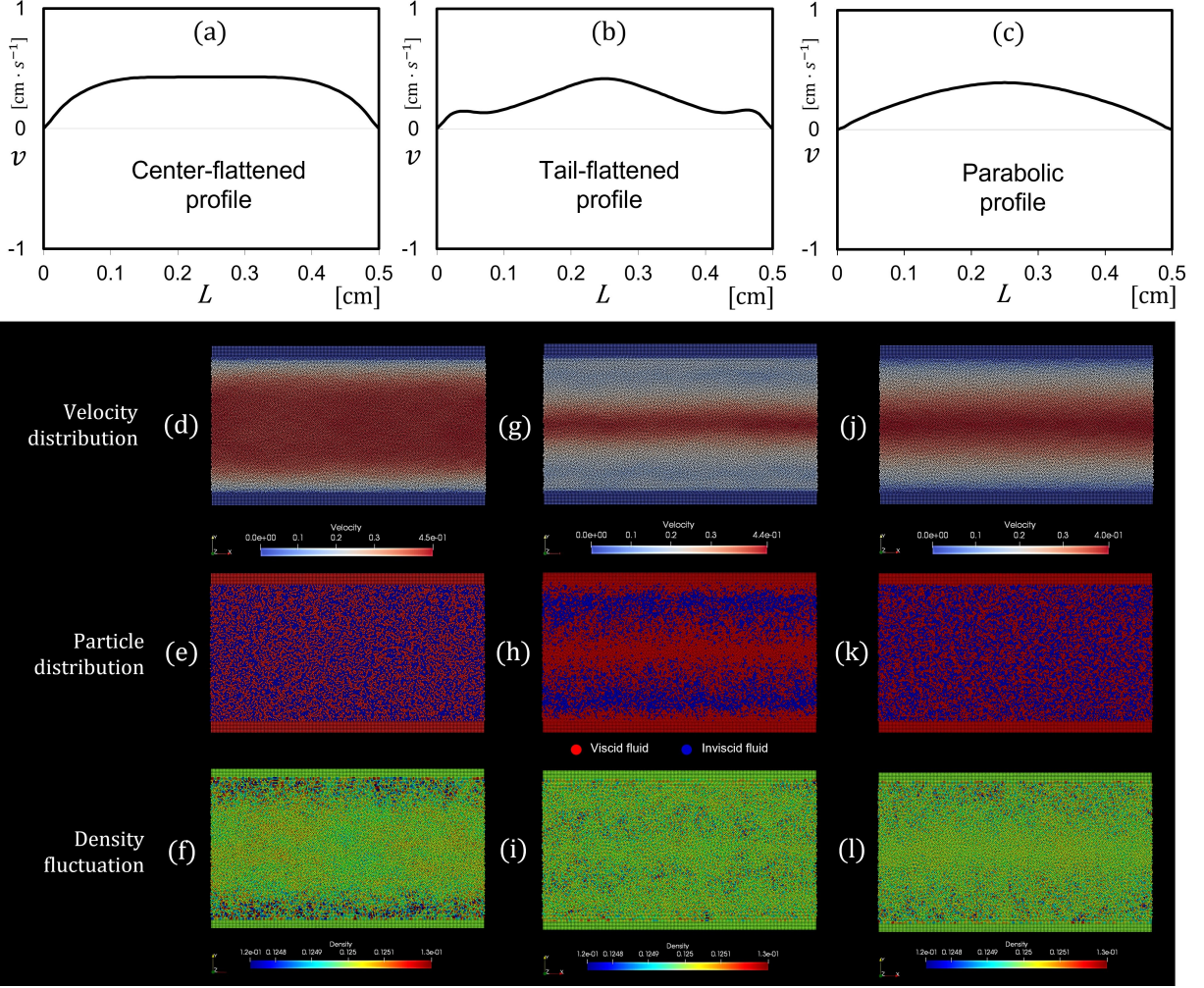


Figure 3: Comparison of the simulation results of the counterflow using our two-fluid model based on classical hydrodynamics, demonstrating that all three representative velocity profiles, (a) center-flattened, (b) tail-flattened, and (c) parabolic, were successfully obtained using only the difference in the initial particle distributions. (d)–(f) Velocity distribution, initial particle distribution, and density fluctuation for the center-flattened profile, (g)–(i) for the tail-flattened profile, and (j)–(l) for the parabolic velocity profile, respectively.

for each fluid particle. Consequently, we succeeded in reproducing the characteristic phenomena of quantum vortex lattices, that is, the rigid rotation of multiple vortices around the central axis of a rotating container that rotates independently without dissipation [28, 36, 47]. Figure 1 presents a snapshot of the replicated simulation reported in Refs. [28, 36] under the same computational conditions. Specifically, Fig. 1(a) shows the intensity distribution of the particle velocity, and it can be observed that the velocity distribution is deformed at the spinning vortex. Figure 1(b) presents an enlarged view of Fig. 1(a), visualizing the direction and intensity of the rotational force of the individual vortices as arrow vectors and color maps, respectively. Figure 2 presents a snapshot of the replicated simulation reported in Ref. [37] under the same conditions, showing liquid helium-4 rotating only in the horizontal direction with a certain thickness. As confirmed by Fig. 2, the problem is not isotropic, assuming a quasi-two-dimensional situation that rotates only in the horizontal direction. This is because, in principle, the interaction of quantum vortices in three-dimensional space must be governed topologically, for example, by Schwarz’s rule [13, 14]. Accordingly, the interactions among the vortices shown in Fig. 2 are incorrect. Nevertheless, we successfully reproduced the generation of multiple spinning vortices. In future studies, we expect that our approach can be extended to three-dimensional dynamics by incorporating appropriate topological control using Schwarz’s rule.

In addition, in Ref. [36], the author simulated a 2D counterflow, which is another representative problem for liquid helium-4 at cryogenic temperatures, and reported the reproduction of not only the parabolic velocity profile, which characterizes the classical Hagen–Poiseuille flow, but also the center-flattened velocity profile, where the center of

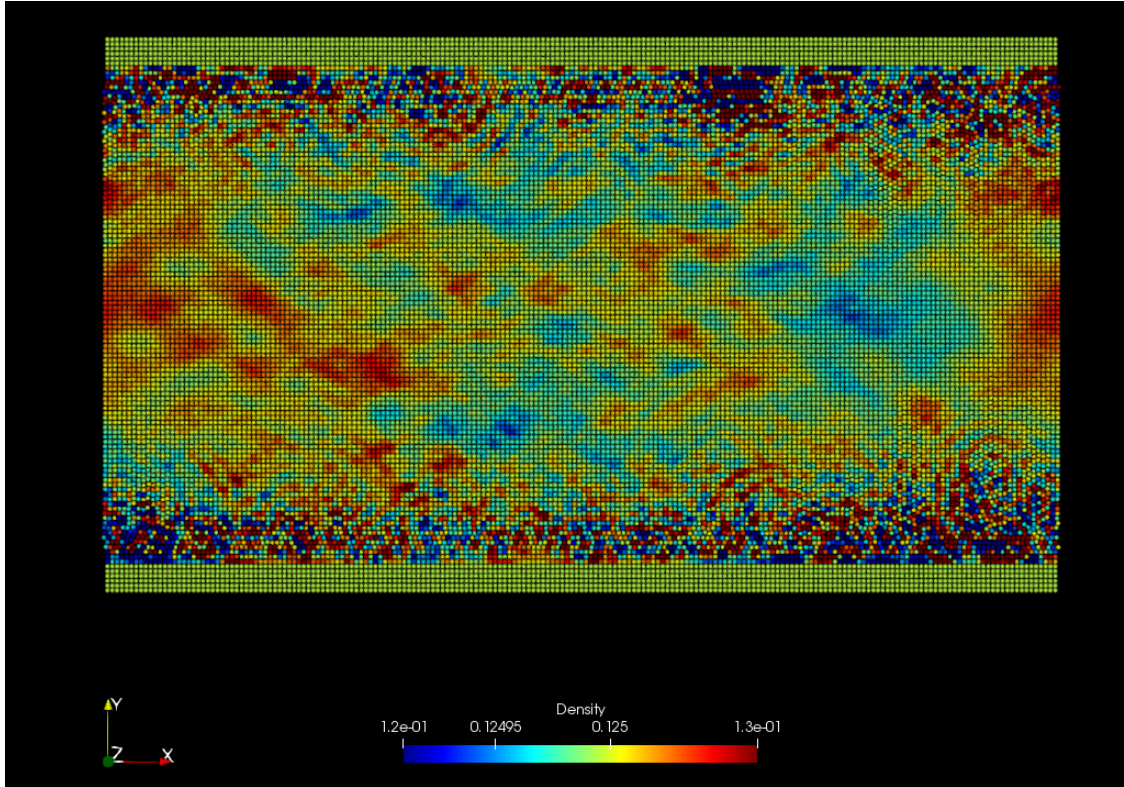


Figure 4: Snapshot of the simulation demonstrating the emergence of shock waves in the explicit SPH calculations, in which a steeper temperature gradient was given to the system, resulting in abrupt and significant density changes occurred in time and space compared with the case in Fig. 3(a). The density oscillation around 1 %, which is not usually emphasized, is intentionally enlarged for clarity (Multimedia view).

the velocity profile is flattened. However, a center-flattened profile can be observed in the Poiseuille flow of classical fluids in turbulent flow regimes; this phenomenon is not unique to quantum fluids. In contrast, a tail-flattened profile, in which the tail portion of the velocity profile near the wall is sluggish and the center portion is raised, has been reported both experimentally and in simulations and is recognized as a phenomenon unique to quantum hydrodynamics. The theoretical explanation for the observed tail-flattened profile is still under debate, but a theory is that it is due to the fact that the superfluid component enters a turbulent flow regime while the normal fluid component is in a laminar flow regime. Recently, it was proposed that, from a microscopic perspective, the spatial distribution of the vortex line density has a significant effect on shaping the center- and tail-flattened profiles [48]. That is, if the generated vortex lines obstruct the flow of the normal fluid component, and if they are uniformly distributed in space, the result is a center-flattened distribution; if they are localized near walls, the result is a tail-flattened distribution. Because vortices do not dissipate in a quantum fluid, the mechanical picture that the spatial structure and distribution of vortices obstruct the flow would be correct. Another point is that the observation time of these vortices in experiments with pulsed lasers is short owing to the decay time (approximately 0.3–3 s according to [49]). Thus, the stationarity of quantum fluids is currently unclear.

As an additional experiment to our previous study [36], we performed counterflow simulations using our two-fluid model and successfully obtained a tail-flattened velocity profile. In our two-fluid model, the residual viscous fluid, which is a low-density component of the two components in the low-temperature regime, forms the cores of the vortices [28]. Thus, we arranged the viscid components such that the spatial distribution of the vortex line density in the initial state in [48] corresponded to that of the viscous component. Further details are as follows: In the cases of the (a) center-flattened profile and (c) parabolic profile, the initial distribution of the viscous component is uniform, and in the case of the (b) tail-flattened profile, the spatial distribution of the vortex line density in Ref. [48] is reflected in the distribution of viscous components, which are concentrated at the wall boundary. In case (c), compared with cases (a) and (b), a temperature difference of a factor of 10 was added at both ends of the system, but the computational conditions were the same for all three cases, (a)–(c). We performed counterflow simulations and, as shown in Figs. 3(a)–(c), we confirmed that we reproduced the three types of velocity profiles observed in the

T	L	Physical space	Discrete space
Finite temperature	Millimeter scale ( $10^{-2}$ m – $10^0$ m)	<p><b>Macroscopic quantum phenomena of cryogenic liquid helium-4 observed at the hydrodynamic scale</b></p> <p>Fontaine, Film flow, Torus flow, Rotational viscosity, Vortex lattice, Hagen-Poiseuille flow, Counterflow</p> <p>Refer to the following for the details of (1) – (5):            Phys. Fluids 36, 087155 (2024)            Phys. Fluids 34, 127116 (2022)            Phys. Fluids 33, 087117 (2021)            J. Phys. Commun. 5, 035001 (2023)</p> <p><b>A. Two-fluid model based on classical fluid dynamics</b></p> $\rho_s \frac{D\mathbf{v}_s}{Dt} = -\frac{\rho_s}{\rho} \nabla P + \rho_s \sigma \nabla T - \mathbf{F}_{Sn} \quad \dots (1)$ $\rho_n \frac{D\mathbf{v}_n}{Dt} = -\frac{\rho_n}{\rho} \nabla P - \rho_n \sigma \nabla T + \eta \nabla^2 \mathbf{v}_n + \mathbf{F}_{Sn} \quad \dots (2)$ <p>Reformulation of the Navier-Stokes equation to conserve spin-angular momentum around the axes of constituent particles (D. W. Condiff, 1964)</p> $\rho_n \frac{D\mathbf{v}_n}{Dt} = -\frac{\rho_n}{\rho} \nabla P - \rho_n \sigma \nabla T + \left( \frac{\eta}{3} + \frac{\xi}{2} \right) \nabla^2 \mathbf{v}_n + \left( \frac{\eta}{3} + \xi - \frac{\eta}{2} \right) \nabla \nabla \cdot \mathbf{v}_n + 2 \frac{\eta}{3} \nabla \times \boldsymbol{\omega}_n + \mathbf{F}_{Sn} \quad \dots (3)$ <p><b>B. Two-fluid model based on quantum hydrodynamics</b></p> $\rho_s \frac{D\mathbf{v}_s}{Dt} = -\frac{\rho_s}{\rho} \nabla P + \rho_s \sigma \nabla T - \mathbf{F}_{Sn} \quad \dots (4)$ $\rho_n \frac{D\mathbf{v}_n}{Dt} = -\frac{\rho_n}{\rho} \nabla P - \rho_n \sigma \nabla T + \eta \nabla^2 \mathbf{v}_n + \mathbf{F}_{Sn} \quad \dots (5)$ <p>Two expressions of the chemical potential</p> $\mu = \frac{V}{N} \nabla P - \frac{S}{N} \nabla T \quad (6)$ $\mu = g n + V_{\text{ext}} - \frac{\hbar^2}{2m\sqrt{n}} \nabla^2 \sqrt{n} \quad (7)$ <p>The two-fluid model in B was obtained by assuming the existence of two components and applying the following conditions (A)–(C) similarly to Newtonian mechanics (I.M. Khalatnikov, 1965); the same derivation can be made for A.</p> <p><b>(A) Energy flux conservation</b></p> $\frac{\partial E}{\partial t} + \nabla \cdot (\mathbf{Q} + \mathbf{Q}') = 0$ <p><b>(B) Relationship from thermodynamics</b></p> $\frac{\partial E}{\partial t} = T \frac{\partial S}{\partial t} + v \frac{\partial p}{\partial t} + v_n \frac{\partial j}{\partial t} - \rho_s W \cdot \frac{\partial \mathbf{v}_s}{\partial t}$ $\left[ \mathbf{W} \equiv \mathbf{v}_s - \mathbf{v}_n, \quad v = \mu + \frac{v_s^2}{2} - v_n \cdot \mathbf{v}_s \right]$ <p><b>(C) The principle of Galilean relativity</b></p> <p>Momentum density <math>\mathbf{J} = \rho \mathbf{v}_s + \mathbf{J}_0</math>, <math>\mathbf{J}_0 = \rho \mathbf{W}</math></p> <p>The subscript 0 indicates the rest frame coordinate system.</p> <p><b>Cf. Microscopic expression of momentum density using the Bogoliubov theory</b></p> <p>From consider the contribution of non-condensate components up to the first order in the expansion of the GP equation, one obtains the following:</p> $\mathbf{j} = \rho \mathbf{v}_s + \mathbf{V} \cdot \sum_{\mathbf{k}} \mathbf{k} n_{\mathbf{k}}$ <p><b>Basic concepts of bosonic many-body systems</b></p> <p>(a) Case with interactions            The Hamiltonian obtained from the second quantization</p> $\hat{H} = \int d\mathbf{r} \hat{\Psi}^\dagger(\mathbf{r}) \left( -\frac{\hbar^2 \nabla^2}{2m} + V_{\text{ext}} \right) \hat{\Psi}(\mathbf{r}) + \frac{1}{2} \int d\mathbf{r} d\mathbf{r}' \hat{\Psi}^\dagger(\mathbf{r}) \hat{\Psi}^\dagger(\mathbf{r}') \hat{\Psi}(\mathbf{r}') \hat{\Psi}(\mathbf{r}) \quad \dots (14)$ <p>(b) Case without interactions            Bose-Einstein Condensation (BEC) Theory</p> $\frac{N_c}{N_c} = \left[ 1 - \left( \frac{T}{T_c} \right)^{3/2} \right]^{-1} \quad \dots (15)$ <p><b>(#) The conservation laws for mass density <math>\rho</math>, momentum density <math>\mathbf{j}</math>, entropy density <math>S</math>, and the motion equation for superfluid velocity <math>\mathbf{v}_s</math> are given below:</b></p> $\frac{\partial \rho}{\partial t} + \nabla \cdot \mathbf{j} = 0 \quad \dots (8)$ $\frac{\partial \mathbf{j}}{\partial t} + \nabla \cdot (\Pi + \Pi') = 0 \quad \dots (9) \quad \rho = \rho_s + \rho_n$ $\frac{\partial \mathbf{v}_s}{\partial t} + \nabla \cdot \left( \phi + \frac{1}{2} \mathbf{v}_s^2 + \mathbf{h}' \right) = 0 \quad \dots (10) \quad \mathbf{j} = \rho_s \mathbf{v}_s + \rho_n \mathbf{v}_n$ $\frac{\partial S}{\partial t} + \nabla \cdot (\mathbf{J}_s + \mathbf{J}_s') = \frac{R}{T} \quad \dots (11) \quad \Pi = P \delta_{ij} + \rho_s v_{si} v_{sj} + P \delta_{ij} + \rho_s v_{si} v_{sj}$ <p>Variables: <math>\mathbf{h}'</math>, <math>\Pi</math>, <math>\mathbf{J}_s</math> and <math>\mathbf{Q}</math> represent unknowns/dissipation terms.</p> <p>Legend:  <math>\rho</math>: Mass density  <math>P</math>: Pressure  <math>T</math>: Temperature  <math>S</math>: Entropy generation rate  <math>w</math>: Velocity of normal fluid  <math>v_s</math>: Velocity of superfluid  <math>\rho_n</math>: Density of normal fluid  <math>\rho_s</math>: Density of superfluid  <math>\mathbf{J}</math>: Scalar quantity (unknown)  <math>\mathbf{J}_s</math>: Entropy flux (unknown)  <math>\mathbf{Q}</math>: Heat flux (unknown)  <math>\mathbf{W}</math>, <math>\mathbf{V}</math>, <math>\mathbf{J}</math> and <math>\mathbf{Q}</math> are unspecified.</p>	<p><b>Smoothed Particle Hydrodynamics (SPH)</b></p> <ul style="list-style-type: none"> <li>Finite particle approximation using the Lagrangian description.</li> <li>The discretization points represent the particles to be observed, which possess properties and embody dynamic characteristics.</li> </ul> <p><b>Finite Difference Method (FDM)</b></p> <ul style="list-style-type: none"> <li>Finite difference approximation based on the Eulerian description.</li> <li>The physical profiles are recorded at fixed points on the rest frame.</li> </ul> <p>Discretization of the two-fluid model (A) or (B) using SPH</p> <p>A list of the SPH operators for discretization</p> <p>Original form vs. Discretized form</p> <p><b>Physical quantity</b> <math>\phi(\mathbf{r}_i) := \sum_j \frac{m_j \phi(\mathbf{r}_j)}{p_j} W( \mathbf{r}_i - \mathbf{r}_j , h)</math></p> <p><b>Gradient</b> <math>\nabla \phi(\mathbf{r}_i) := \rho_i \sum_j \frac{m_j}{p_j} \left( \frac{\phi(\mathbf{r}_j) - \phi(\mathbf{r}_i)}{ \mathbf{r}_j - \mathbf{r}_i } \right) \frac{\mathbf{r}_j - \mathbf{r}_i}{ \mathbf{r}_j - \mathbf{r}_i } \nabla W_{ij}</math></p> <p><b>Laplacian</b> <math>\nabla^2 \phi(\mathbf{r}_i) := \sum_j \frac{m_j \phi(\mathbf{r}_j) - \phi(\mathbf{r}_i)}{p_j} \left( \frac{\mathbf{r}_j - \mathbf{r}_i}{ \mathbf{r}_j - \mathbf{r}_i } \right) \cdot \nabla W_{ij}</math></p> <p><b>Rotation</b> <math>(\nabla \times \mathbf{C})_i := -\sum_j \frac{m_j \mathbf{C}_j}{p_j} (\mathbf{G}_i + \mathbf{G}_j) \times \nabla W_{ij}</math></p> <p>The differential operators act on the kernel function or its derivative.</p> <p>Discretization of Equations (13) or (14) using SPH</p> <p>SPH provides a unified framework in the discrete space because all the term can be expressed in one of the forms: <math>(+)\nabla W_{ij}</math>, <math>(+)\nabla W_{ij}</math>, <math>(-)\nabla W_{ij}</math>, or <math>(+)\nabla W_{ij}</math>.</p>
	Finite temperature	Nanometer scale ( $10^{-9}$ m)	
Absolute zero	Atomic size Angstrom scale ( $10^{-10}$ m)		

Figure 5: Schematic of the theoretical models representing the dynamics of liquid helium-4, which are closely associated with our two-fluid model based on classical hydrodynamics, classified by temperature and spatial scale in physical and discrete space, summarized on a single page and embedded in vector form for easy enlargement. The correspondence between the fourth and fifth terms on the right side of Fig. 5(3) with the divergence of the subgrid scale stress tensor  $(-\nabla \cdot \boldsymbol{\tau}_{SGS})$  is presented in Sec. 3.2.

cryogenic liquid helium-4. In particular, the (b) tail-flattened velocity profile is unique to quantum fluids. Notably, using a two-fluid model based on classical hydrodynamics, we were able to reproduce the tail-flattened velocity profile based only on the differences in the spatial distribution of the particles. Each row in Fig. 3 corresponds to results (a), (b), and (c). For example, Figs. 3(d), (g), and (j) show velocity profiles in the spatial directions corresponding to (a), (b), and (c), and (a)–(c) are averages of these projections in the x direction. Snapshots taken at comparable velocities are shown for comparison in (a)–(c). Figures 3(e), (h), and (k) show the spatial distributions of the two components corresponding to (d), (g), and (j), respectively. It can be observed that the initial difference in particle distribution is maintained after a certain time. Furthermore, the density oscillates by a few percent in the SPH simulations with an explicit time-integrating scheme. Figures 3(f), (i), and (l) show the spatial distribution of the density corresponding to (a), (b), and (c), respectively, where the color map is given in the range of a 4 % variation with respect to the mean value. Thus, fluctuations of less than 3 % become pronounced. A comparison of the velocity profiles with the density fluctuation profiles for each of the three velocity profiles confirmed that the velocity tended to be lower where the density fluctuations were larger. Density fluctuations of up to 0.2 % in the relative error to the mean were observed for the (b) tail-flattened and (c) parabolic profiles, and up to approximately 0.35 % for the (a) center-flattened profile. The reason for the larger fluctuations in (c) is that a 10-fold temperature gradient was applied in (c). It should be emphasized that the two-fluid model based on classical hydrodynamics was used to confirm the tail-flattened velocity profile based only on the difference in the spatial distribution of the particles. In summary, we succeeded in reproducing phenomena previously considered unique to quantum fluids in both vortex lattice and counterflow problems using a two-fluid model based on classical hydrodynamics.

Furthermore, in simulations of incompressible flows using SPH, one can occasionally observe a shockwave owing to density fluctuations. In other words, if there are abrupt and significant density changes in time and space, the flow velocity instantaneously exceeds the allowable maximum velocity determined by the Courant–Friedrichs–Lewy (CFL) condition [50], and the system breaks the continuum approximation condition, generating shockwaves. Figure 4 shows the results of the simulation in which the computational conditions were set such that the maximum velocity of the fluid particles approached the allowable maximum velocity by imposing a steeper temperature gradient than that in the case in Fig. 3(a). In Fig. 4, the maximum density oscillation was approximately 1.1 % and we confirmed the generation of a shockwave (see the multimedia view). In computational fluid dynamics, exceptional phenomena that fall outside the scope of the continuum hypothesis are abhorred in incompressible classical fluid simulations because

they do not ensure complete incompressibility. The nature of shockwave generation observed in the case of SPH with an explicit time-integrating scheme has often been considered a disadvantage for simulating incompressible classical fluids; accordingly, it has been neglected. The calculation diverges when shockwaves occur in methods other than SPH. However, in liquid helium-4 at cryogenic temperatures, oscillatory phenomena with respect to the pressure or density can be observed, which is the so-called first sound wave. In summary, SPH can reproduce sound waves similar to those of liquid helium-4 at cryogenic temperatures.

These recent numerical simulation results raise the question of why the SPH formulation makes it possible to reproduce several macroscopic quantum phenomena thought to be caused by the microscopic changes in physical properties represented by the loss of molecular viscosity by solving a two-fluid model based on classical hydrodynamics. This paper aims to provide a convincing explanation to this question. In the following sections, we clarify the significance and position of our two-fluid model based on classical hydrodynamics by comparing it with the related quantum hydrodynamic theories. Our simulation results suggest that the discretized form of SPH has a “reverse coarse-graining effect.” Regarding this point, we show that solving the two-fluid model based on classical hydrodynamics using SPH can reproduce the fluctuations at the microscopic scale because the truncation errors owing to the smoothing kernel approximation can substitute the fluctuations at the microscopic scale. In particular, the fluctuations can be reproduced at more macroscopic scales and are amplified according to the size of the kernel radius. We also consider the possibility that two-fluid models based on classical and quantum hydrodynamics have a relationship between the scale transformation by filtering in the large eddy simulation (LES) and the inverse scale transformation by SPH. We also discuss that the spin angle momentum conservation term, which we previously introduced into the two-fluid model as a quantum mechanical correction, formally corresponds to the subgrid -scale (SGS) model, which can be derived from the scale transformation of the two-fluid model from quantum to classical hydrodynamics. Our results and discussion provide new insights into the microscopic composition of cryogenic liquid helium-4 in a multiscale framework and serve as a basis for future research. In other words, a normal fluid can be a mixture of inviscid and viscous particles. Second, a flow identified as a normal fluid on the microscopic scale because of the presence of molecular viscosity is still classified as an inviscid fluid on the hydrodynamic scale because its viscosity is insufficient to produce eddy viscosity. The remainder of this paper is organized as follows: Section 2 reviews our two-fluid model to clarify its significance and position with respect to related methods and theories within the framework of multiscale physics. In Section 3, we discuss the inverse coarse-graining effects of SPH. In particular, we demonstrate the relationship between spatial filtering in LES and smoothing in SPH, showing that they serve as the scale and inverse scale transformations of the two-fluid models based on classical and quantum hydrodynamics, while arguing for the correspondence between the viscosity correction term to conserve the spin angular momentum and SGS model. Section 4 summarizes the conclusions of this study.

## 2. Cryogenic liquid helium-4 in the framework of multiscale physics

Figure 5 shows a schematic of the theoretical models representing the dynamics of liquid helium-4, which are closely associated with our two-fluid model based on classical hydrodynamics. The models are classified by temperature and spatial scale in physical and discrete spaces, summarized on a single page, and embedded in a vector form for easy enlargement. The two-fluid model based on classical hydrodynamics is shown in Fig. 5(1)–(3) next to the letter A, which is highlighted in red. It should be noted that an independent version of Fig. 5 is provided in the Supplementary Material.

### 2.1. Microscopic description of liquid helium-4: from Bose–Einstein condensates to quantum hydrodynamics

Let us start with the case without interactions in (b), where the basic concepts of bosonic many-body systems are shown at the bottom of Fig. 5. As mentioned in the Introduction, liquid helium-4 is a bosonic many-body system. The most fundamental concept for describing liquid helium-4 is the ideal Bose gas, which ignores the interactions between bosons and focuses on their quantized energy states, assuming that the number of particles occupying a given energy state is unlimited. In addition, no distinction can be made between the individual particles. The statistics of bosonic particles described under these conditions can be calculated using basic quantum statistical mechanics [51]. The relationship between the expected value of the ratio of the number of particles  $N_s$  that can assume the energy ground state in thermal equilibrium at a certain temperature  $T$  and the total number of particles  $N_t$ , temperature  $T$ ,

and critical temperature  $T_B$  is shown in Fig. 5(15). Next, let us consider Fig. 5(b), that is, the case of interactions between particles. If the particle interaction potential is given by a symmetric two-body potential, we can derive the specific expression of the Hamiltonian via a “second quantization” as shown in Fig. 5(14). Here, the second quantization is a procedure to extend the operators of creation and annihilation so that these operators and their eigenvalues for all possible states can be defined at arbitrary locations in space; the extended operators are then called field operators. Specifically, a field operator for creation at location  $\mathbf{r}$  is obtained by linearly combining the eigenfunctions of all possible states at this location with the respective creation operators. Briefly, the field operator for creation determines the expectations of the creation operators for all possible states at location  $\mathbf{r}$ . The same discussion applies to annihilation operators. The second quantization of the field allows us to define the particle number density in space. For a detailed description of the second quantization, please refer to Refs. [52–54]. It is not necessary here to understand the specific expressions of Fig. 5(14) and (15)). It is sufficient to know that liquid helium-4 at near absolute zero portrays such a quantum mechanical picture, in principle. At finite temperatures, some Bose particles are excited; they are classified into two components: condensed components in the energy ground state and non-condensed components in the excited states. Figure 5(14) provides a general description of the Hamiltonian for the entire system when considering the particle–particle interactions. Two approximations: (i) the Bogoliubov approximation [55], which neglects the contribution of the noncondensable component, and (ii) an approximation that allows for the locality of the particle interaction and replaces the symmetric two-body potential with a Dirac delta function as shown in Fig. 5(13), yield the Gross–Pitaevskii (GP) equation [56, 57], whose detailed expression is represented in Fig. 5(12). The GP equation is a nonlinear Schrödinger equation for boson systems and is the time evolution equation of the wave function of the condensate. Although the GP equation provides an explanation for the essential mechanism of liquid helium dynamics, it cannot quantitatively reproduce the detailed behavior of the strongly interacting liquid helium because it assumes (ii) a local interaction approximation, as mentioned above. Therefore, a different approach is required.

In the derivation of the GP equation, the contribution of the noncondensed component is neglected by the Bogoliubov approximation in (i). Although this may be acceptable near absolute zero, there is a certain amount of excited (i.e., non-condensed) components at finite temperatures. In the noncondensed components, the molecular viscosity is revived owing to reactivated interatomic interactions, which have been lost in the energy ground state. Two types of flows exist at finite cryogenic temperatures: a non-viscous flow composed of condensed components, and a mean flow of components that have acquired viscosity owing to excitation, that is, normal fluid components. In 1965, I.M. Khalatnikov recognized the existence of the two components and derived a two-fluid model based on the following three relationships established in Newtonian mechanics: (A) the conservation of the energy flux, (B) the time evolution equation of energy derived from the first law of thermodynamics, and (C) the Galilean principle of relativity between the two components [58]. An overview of Khalatnikov’s derivation of the two-fluid model is presented in Fig. 5, which is highlighted in yellow. The resulting two-fluid model is illustrated in Figs. 5(4) and (5). It is referred to as the two-fluid model based on quantum hydrodynamics, which is obtained as follows: By substituting Figs. 5(8)–(11) and (C) into (B) and comparing both sides term-by-term with (A), we obtain the following expressions for the scalar function  $\phi$  and entropy flux, which are unknown in the equations:  $\phi = \mu$  and  $\mathbf{J}_S = S\mathbf{v}_n$ . Figs. 5(8)–(11) represent the conservation law of mass density, the conservation law of momentum density, the equation of motion of the superfluid component, and the conservation law of entropy, respectively. Figs. 5(8)–(11) contain, in addition to  $\phi$  and  $\mathbf{J}_S$ , four other unknown parameters that give rise to the dissipative effects:  $\Pi'$ ,  $h'$ ,  $\mathbf{J}'_S$ , and  $Q'$ . In total, there are six unknowns. However,  $\Pi'$ ,  $h'$ ,  $\mathbf{J}'_S$ , and  $Q'$  cannot be specified, because only two equations are obtained by comparing both sides of (A) and (B) term-by-term after substituting Figs. 5(8)–(11) and (C) into (B). The expression for the viscosity term in the two-fluid model is yet to be determined. Hence, even for the quantum-hydrodynamics-based two-fluid model in B, the dissipative terms  $\Pi'$ ,  $h'$ , and  $Q'$  are usually given by assuming classical Newtonian fluids where the symmetric component of the stress tensor depends only on the symmetrized velocity gradient tensor. In addition, Fourier’s law,  $\mathbf{J}'_S = -\nabla T$ , is assumed as in classical hydrodynamics.

It is important to emphasize that the laws in the derivation of the two-fluid model are common to Newtonian dynamical systems. Specifically, in Fig. 5, the conservation law of energy in (A), the time evolution equation of energy derived from the first law of thermodynamics in (B), Galilean relativity in (C), the conservation law of mass density in Fig. 5(8), and the conservation law of momentum density in Fig. 5(9) are common to classical dynamical systems. In contrast, of the two resulting relations,  $\phi = \mu$  and  $\mathbf{J}_S = S\mathbf{v}_n$ , the entropy density relation  $\mathbf{J}_S = S\mathbf{v}_n$  is unique to cryogenic liquid helium-4, indicating that only the normal fluid component transports entropy. However,

this physical picture also holds true within the framework of classical inviscid and viscous flows. Moreover, the physical picture of the interaction between the two components is not related to the derivation of the two-fluid model. Originally, the two components were thought to exist independently; however, mutual friction was later introduced between them by Gorter and Mellink [11]. Nevertheless, the mutual friction force acts in the opposite direction of the two components, and thus, they cancel each other out. Therefore, it is reasonable to conclude that it does not affect the conservation law of the two-fluid model. Even if there are non-negligible contributions owing to mutual friction effects, these frictional effects can be understood to be included in  $\Pi'$ ,  $h'$ , and  $Q'$  because the two-fluid model leaves the arbitrary of the dissipative terms, as mentioned above. In summary, the two-fluid model is an incomplete system that leaves the arbitrary in the dissipative terms and the physical picture of the interaction between the two components. These incomplete features can be exploited to extend the two-fluid model to multiscale physics.

## 2.2. *Macroscopic description of liquid helium-4: the two-fluid model based on classical hydrodynamics*

As mentioned in the Introduction, the goal of our project was to numerically reproduce fluid phenomena (e.g., torus flow) specific to bulk liquid helium-4, which are often described as macroscopic quantum phenomena. From the viewpoint of computational resolution, it is not realistic to describe these fluid phenomena, which can be observed with the naked eye, based on quantum fluid equations covering the nanometer and micrometer spatial scales. It is clearly more feasible to reproduce them using the NS equations, which are the governing equations on the same spatial scale as the fluid phenomena under investigation. Based on this viewpoint, liquid helium-4 can be regarded at cryogenic temperatures as a mixture of inviscid and viscous fluids, and the viscous fluid component remains in the inviscid fluid at finite temperatures. As the temperature decreases, the viscous fluid component decreases, and at absolute zero, it is assumed to be a single-phase flow of inviscid fluid. In addition, we assume the classical weakly compressible flow, i.e., quasi-incompressible flow, because of the following two concepts in quantum statistical mechanics: (1) the ratio of the two components, superfluid and normal fluid, is a statistical mean value and instantaneously fluctuates around the mean, and (2) the component that causes BEC in bulk liquid helium is at most 13 % of the total, even at absolute zero [59]. We adopted SPH because it allows for weak compressibility while simultaneously satisfying the incompressibility condition. The SPH allowed us to introduce the following particle corrections: First, the independent variable of temperature  $T$  fluctuates around its mean because we obtain  $T$  as a statistical average among neighboring particles by a weighted calculation, even if we do not solve the time-evolution equation for this variable. Thus, both the density and temperature fluctuate around the mean. This fluctuation can induce an instant temperature gradient force in the vicinity of the interface between the two fluids, even if the temperature is uniform from a macroscopic perspective, thereby generating interfacial tension between the two components in opposite directions. This interface effect can be ignored if the fluctuations are moderate and continuity is maintained. However, if the two components are excessively close to each other near the interface, a steep gradient is produced, and the interfacial tension becomes non-negligible. This property can be assumed to appear in the induced direction in exceptional scenarios in which significant particle inhomogeneity occurs owing to external impacts or heat addition. In addition, the local interaction force between the two components can be considered, which is proportional to the velocity difference between the two components by reference to the fluid–particle interactions in the multiphase flows [60–62].

We developed a two-fluid model that a) consists of two components, classical inviscid and viscous fluids, b) has an interfacial tension between the two components that is induced only under specific conditions, and c) has a local interaction force between the two components that is proportional to the velocity difference near the interface [28, 36, 37, 47]. In summary, our model is a conventional two-phase flow model described in a Lagrangian manner, except for the constraint on the conditions and direction of the interfacial tension generation in (b). The formula for our two-fluid model based on classical hydrodynamics is shown in Figs. 5(1)–(3) next to the letter A, highlighted in red at the top of the figure. We refer to the fluid components described in Figs 5(1) and (2) as “inviscid fluid” and “viscid fluid,” respectively, in contrast to the terms “superfluid” and “normal fluid” for the two components in Figs 5(4) and (5). We originally named Figs 5(1) and (2) as “superfluid” and “normal fluid” at the early stage of our studies [28, 36, 47]. However, we decided to change these names later to clarify the differences in spatial scaling. It is important to note that the specific formulae in Figs. 5(1) and (2) are consistent with those shown in Figs. 5(4) and (5) of the two-fluid model based on quantum hydrodynamics. The reason for this is clear because, as mentioned above, the derivation of the two-fluid model only assumes the following laws, which are naturally defined in the Newtonian dynamical system: (A) the law of conservation of energy flow velocity, (B) the time evolution equation of energy derived from the first law of thermodynamics, (C) the Galilean relativity principle between two components, as well as the three

conservation laws for mass, momentum, and entropy densities and the equation of motion for one of the components, which are presented in (8)–(11). Moreover, the physical picture of the interaction between the two components can be irrelevant to the derivation of the two-fluid model with mutual interaction, as long as they cancel in opposite directions in the same manner as the basis for introducing mutual friction in the two-fluid model in B. Accordingly, we can derive Figs. 5(1)–(2) of our two-fluid model by simply replacing the “superfluid” with “inviscid fluid” and “normal fluid” with “viscous fluid,” and redefining the local physical quantities such as  $\rho_s$ ,  $\rho_n$ , and  $\mu$  of the superfluid or normal fluid components as the corresponding physical quantities of the inviscid and viscid fluids defined for the macroscopic domains.

Figure 5(3) is a re-derivation of the viscosity term inspired by Condiff’s work for polar fluids [45], which reformulated the NS equation to explicitly represent the degrees of freedom of the constituent particles, resulting in the viscosity term being decomposed into shear viscosity  $\mu$ , bulk viscosity  $\bar{\xi}$ , and rotational viscosity  $\bar{\mu}_r$ . The fifth term on the right-hand side includes the parameter  $\omega_0$ , which represents the internal degrees of freedom of a molecular particle, corresponding to the rotational angular velocity around the axis of the particle if the particle can be considered a spherical rigid body. In this case,  $\omega_0$  makes it possible to preserve the rotational velocity around the axis, that is, the spin angular velocity of each constituent particle, by setting  $\omega_0$  to a constant value. Although  $\omega_0$  was originally a parameter defined for molecules, it has been recognized through experiments and simulations as a parameter defined for virtual fluid particles based on the coarse-graining concept [46]. The conservation of the spin angular momentum shown in Fig. 5(3) may allow the system to approach quantum hydrodynamic systems because it can ensure the quantization of the angular momentum per constituent particle. In other words, ensuring the quantization of the spin angular velocity in the local fluid field governing the vortex dynamics may bring the fluid system closer to a quantum hydrodynamic system. At present, this hypothesis is tentative; however, the recent results of our calculations on vortex lattices and counterflows, that is, the solution of a spinning angular momentum-conserving two-fluid model using SPH, which reproduced the velocity profiles in vortex lattice phenomena and counterflow problems previously thought to be phenomena unique to quantum hydrodynamics, support this hypothesis. For more details of the derivation and physical interpretation of Fig. 5(3), see Section II.A and Fig. 9 in Ref. [37]. Its use in the two-fluid model of cryogenic liquid helium-4 for the 2D problem is presented in Refs. [28, 36, 47]. The reformulation of the NS equations by D. Condiff is found in Ref. [45], and its SPH discretization is provided in Ref. [46].

We now discuss the difference in the physical significance of the physical parameters density  $\rho$  and viscosity  $\mu$  between these two two-fluid models based on the classical hydrodynamics of Figs. 5(1) and (2) and the quantum hydrodynamics of Figs. 5(4) and (5)). Because the density is defined as the mass per unit volume, it can be considered the same between the two-fluid model of quantum hydrodynamics and the two-fluid model based on classical hydrodynamics. Note that the density can only be defined after the field operators and the local average of the physical quantities are introduced; thus, it can only be defined at the spatial scales at which they are introduced, i.e., the scale larger than the scale at which the GP equation is defined. On the other hand, the physical significance of the viscosity coefficient differs between the two-fluid models. The viscosity coefficient  $\bar{\mu}$  of Fig. 5(2) (or  $\bar{\mu}$ ,  $\bar{\xi}$ , and  $\bar{\mu}_r$  in Fig. 5(3)) in the two-fluid model based on classical hydrodynamics is defined as the ratio of the velocity gradient to stress; thus, this is a parameter in continuum mechanics. In contrast, the viscosity coefficient  $\mu$  of the two-fluid model based on quantum hydrodynamics is a microscopic parameter in the transitional flow or free molecular flow regimes dominated by the Boltzmann equation rather than the classical hydrodynamic regime in which the NS equation is dominant. By reference to Maxwell’s theory [63–65], the viscosity coefficient  $\mu$  for an ideal gas can be expressed as  $\mu = \rho\lambda\sqrt{v^2}/3$ , where  $\rho$  is density,  $\lambda$  is the mean free path, and  $\sqrt{v^2}$  is the root mean square (RMS) velocity of the molecules. Therefore, the definition of the viscosity coefficient differs between the microscopic and macroscopic systems. Nevertheless, because the physical (molecular) viscosity is an inherent property of a substance, the values of the viscosity coefficients in Figs. 5(2) and (5) are expected to be the same ( $\mu = \bar{\mu}$ ). From a kinetics perspective, the eddy viscosity coefficient can serve as an indicator of the apparent viscosity of complex fluid phenomena with a high Reynolds number on a macroscopic scale. Elucidating the conditions under which a system transitions to a turbulent state can offer insights into the dynamic properties of large-scale liquid helium-4. As a preliminary step for future research, the following section clarifies the relationship between the two-fluid models at different scales from the perspective of multiscale physics.

### 3. Discussion

There is a clear distinction between vortex dynamics in the classical and quantum hydrodynamic regimes; in the former, vortices dissipate, whereas in the latter, vortices do not dissipate and exist in a stable state because the circulation is quantized. The large vortices observed on the spatial scale of classical hydrodynamic cascade into smaller vortices. At this time, energy passes from the larger vortex to the smaller vortex. Eventually, when the vortex size reaches the Kolmogorov microscale [66, 67], it dissipates and disappears owing to molecular viscosity. While larger vortex sizes tend to exhibit characteristics specific to individual problems, as the vortex size decreases, the vortex becomes more universal in nature, independent of dissipation and external forces. The regime in which such vortices are observed is called a universal subrange; in particular, the inertia-dominated regime is called an inertial subrange zone [66, 68]. However, small vortices sometimes merge to form large vortices known as inverted cascades. In other words, from a macroscopic perspective, vortex dynamics are a statistical phenomenon. In general, in a uniform and isotropic classical fluid, the relationship between the vortex energy spectrum  $E$  and wavenumber  $k$  is  $E(k) = k^{-5/3}$  in the inertial regime (Kolmogorov's  $-5/3$  law) [69, 70]. In quantum hydrodynamics, vortices do not dissipate because the circulation is quantized as previously mentioned. However, the energy transfer mechanism is similar to that of classical fluid systems, especially in inertial subrange zones, where the Kolmogorov's  $-5/3$  law has been verified in recent studies. In other words, the property observed in classical fluid dynamics, cascade splitting from large vortices to small vortices and the accompanying energy transfer, is also a common property in quantum fluid dynamics under certain conditions. In summary, the flow structures in the classical and quantum hydrodynamic regimes exhibit certain common properties.

In the hydrodynamic domain, where the spatial scale is smaller than the Kolmogorov scale, the eddies disappear owing to heat dissipation by the molecular viscosity. Unfortunately, this explanation does not hold for quantum fluids such as liquid helium-4 at cryogenic temperatures, where the molecular viscosity can be neglected, even at spatial scales smaller than the Kolmogorov microscale. In other words, it is not yet clear how the turbulent structure in classical hydrodynamics is connected to the turbulent quantum structure in the quantum hydrodynamic regime, where quantum eddies are stable and do not dissipate. In other words, how eddy energy transfer and splitting or coupling are altered in the transition region from the classical to the quantum hydrodynamic scale is not known in detail. However, the space-time diagram in Fig. 5 shows the following facts that are important for elucidating the multiscale physics of liquid helium-4. In the fluid problem of bulk cryogenic liquid helium-4, the governing equations of fluid phenomena can be uniquely described by a two-fluid model at any spatial scale. In fact, the two-fluid model consisting of (1)–(2) and (4)–(5) differs only in the spatial scale, which is not explicitly expressed in the system of equations. Meanwhile, (3) is indispensable for obtaining quasi-quantum effects at the spatial scale of classical fluid mechanics. Here, we discuss the relationship between the two-fluid model based on quantum hydrodynamics, consisting of Eqs. (4)–(5), and the two-fluid model based on classical hydrodynamics, consisting of Eqs. (1)–(3). Specifically, we show that the two-fluid models based on classical and quantum hydrodynamics have a relationship between the scale transformation by filtering in LES and inverse scale transformation by SPH. In addition, we show that the spin angle momentum conservation term, which we previously introduced into the two-fluid model as a quantum mechanical correction, formally corresponds to the SGS model, which can be derived from the scale transformation of the two-fluid model from quantum to classical hydrodynamics. Furthermore, we argue that solving the two-fluid model based on classical hydrodynamics using SPH can reproduce the fluctuations at the microscopic scale because the truncation errors caused by the smoothing kernel approximation can substitute the fluctuations at the microscopic scale. The fluctuations can be reproduced and amplified according to the kernel radius, producing quantum-like effects even at more macroscopic scales. We then discuss new insights into the microscopic composition of the cryogenic liquid helium-4 in a multiscale framework. First, a normal fluid can be a mixture of inviscid and viscous fluid particles. Second, a flow identified as a normal fluid on the microscopic scale because of the presence of molecular viscosity is still classified as an inviscid fluid on the hydrodynamic scale because its viscosity is insufficient to produce eddy viscosity.

#### 3.1. Correspondence between spatial filtering in LES and kernel approximation in SPH

In LES, the physical quantity  $f$  is decomposed into the resolved (filtered) component  $\bar{f}$  and the fluctuation component  $f_\epsilon$ :

$$f = \bar{f} + f_\epsilon, \quad (1)$$

where the resolved component  $\bar{f}$  is obtained via spatial filtering as follows [71]:

$$\bar{f}(\mathbf{r}, t) \equiv \int f(\mathbf{r}', t) G(\mathbf{r} - \mathbf{r}', \Delta) d\mathbf{r}'. \quad (2)$$

Here, we omit the position  $\mathbf{r}$  and time  $t$  in Eq. (2) for easy explanation. A simple calculation using Eq. (2) reveals the following properties with respect to  $\bar{f}$  and  $f_\epsilon$  [72–74]:

$$\frac{\partial \bar{f}}{\partial x_i} = \frac{\partial f}{\partial x_i}, \quad \bar{\bar{f}} \neq \bar{f}, \quad \bar{f_\epsilon} \neq 0. \quad (3)$$

The properties in Eq. (3) epitomize the filtering operations in the LES, which differs from the ensemble average used in the Reynolds-averaged Navier-Stokes (RANS) equation [75]. In addition,  $G(\mathbf{r} - \mathbf{r}', \Delta)$  in Eq. (2) represents a filter function with width  $\Delta$  that satisfies the normalization condition  $\int G(\mathbf{r} - \mathbf{r}', \Delta) d\mathbf{r}' = 1$ . An example of  $G$  is the Gaussian, which is expressed as

$$G(\mathbf{r} - \mathbf{r}', \Delta) := \frac{C}{\Delta^m} e^{-(\mathbf{r} - \mathbf{r}')^2 / \Delta^2}, \quad (4)$$

where  $C$  represents a normalization factor, and  $m$  indicates the dimension ( $m = 1, 2, \text{ or } 3$ ).

In SPH, a physical quantity  $f$  expressed in integral form using the Dirac delta function can be approximated by replacing the delta function with a kernel function  $W$ , which is a smoothing function with a width of  $h$ :

$$f(\mathbf{r}, t) = \int f(\mathbf{r}', t) \delta(\mathbf{r} - \mathbf{r}') d\mathbf{r}' \simeq \int f(\mathbf{r}', t) W(\mathbf{r} - \mathbf{r}', h) d\mathbf{r}'. \quad (5)$$

The kernel function  $W$  must satisfy the normalization condition  $\int W(\mathbf{r} - \mathbf{r}', h) d\mathbf{r}' = 1$ . Additionally,  $W$  must be an even function as  $W(\mathbf{r}) = W(-\mathbf{r})$ . There are several types of kernel functions that satisfy these conditions [76, 77]. The Gaussian function is an example of the kernel function. Polynomial functions are preferred for several problems because of the compact support property, where the kernel function becomes zero at an integer multiple of  $h$ .

We can estimate the approximation error of replacing the second equation with the third equation in Eq. (5) as follows. For explanation, let us express the second equation as  $f$  because it describes the true value, and the third equation as  $\bar{f}$  because it represents a filtered value of  $f$  by the kernel function  $W$ , as follows:

$$f := \int f(\mathbf{r}') \delta(\mathbf{r} - \mathbf{r}') d\mathbf{r}', \quad (6)$$

$$\bar{f} := \int f(\mathbf{r}') W(\mathbf{r} - \mathbf{r}', h) d\mathbf{r}'. \quad (7)$$

Here, we omit the position and time on the left-hand sides of Eqs. (6) and (7). In the one-dimensional case, the Taylor expansion of  $\bar{f}$  yields the following [78]:

$$\bar{f} = M_0 f - h M_1 f^{(1)} + h^2 \frac{M_2}{2} f^{(2)} - \dots, \quad (8)$$

where  $f^{(k)}$  is the  $k$ th derivative of  $f$ , and  $M_k$  represents the  $k$ th moment of kernel  $W$  expressed as

$$M_k = \int r^k W(r) dr, \quad (9)$$

where  $r = \frac{x-x'}{h}$  in the  $x$  direction in the one-dimensional problem.  $M_0$  is always 1 because of the normalization condition  $\int W(r) dr = 1$ . Therefore, we obtain the following relationship:

$$\bar{f} = f - h M_1 f^{(1)} + h^2 \frac{M_2}{2} f^{(2)} - \dots, \quad (10)$$

where the odd terms always vanish because  $M_k$  becomes zero when  $k$  is odd. Equation (10) can be extended to a general form in multiple dimensions as follows [79, 80]:

$$\bar{f} = f + \sum_{l=1}^{\infty} \frac{1}{l!} \nabla^{(l)} f(\mathbf{r}) \text{ ::: } \cdots : \int (\hat{\mathbf{r}} - \mathbf{r})^l W(\mathbf{r} - \hat{\mathbf{r}}, h) d^m \hat{\mathbf{r}} \quad (11)$$

$$= f + f_{\epsilon}^{\text{SPH}}. \quad (12)$$

Here, the symbol “:::  $\cdots$  :” represents the  $l$ th order inner product, and  $m$  indicates the dimension ( $m = 1, 2$ , or  $3$ ). We have denoted the second term on the right-hand side of Eq. (11) as  $f_{\epsilon}^{\text{SPH}}$  in Eq. (12). Notably, the arguments in Eqs. (7)–(12) remain valid when the kernel function  $W$  is replaced with  $G$ . This is because only the normalization condition of the  $n$ th-order differentiability is required for  $W$  and  $G$  as filter or smoothing functions, and imposing this condition does not restrict the selectivity of  $W$  and  $G$ .

We describe  $f_{\epsilon}$  in Eq. (1) as  $f_{\epsilon}^{\text{LES}}$ . The expansion of Eq. (2) in the Taylor series, as in Eq. (7), leads to Eq. (11) by replacing  $W$  with  $G$ . Here,  $W = G$  holds true when the Gaussian is designated to both of them; in this case,  $f_{\epsilon}^{\text{SPH}} = -f_{\epsilon}^{\text{LES}}$  is established. In summary, the following relationships were obtained:

$$f = \bar{f} + f_{\epsilon}^{\text{LES}} \quad (13)$$

$$\bar{f} = f + f_{\epsilon}^{\text{SPH}} \quad (14)$$

A previous study has indicated that SPH can be reinterpreted as a filtering of the LES [81]. This study admits the mathematical equivalence between the smoothing of the SPH and filtering of the LES, and we present a new physical interpretation of both in multiscale physics of the cryogenic liquid helium-4: First, Eq. (13) represents the transformation equation in the LES from microscopic to macroscopic scale. The profile is a true value  $f$  that follows the governing equations at a small scale. Filtering eliminates the fluctuation  $f_{\epsilon}^{\text{LES}}$  at the small scale by smoothing  $f$ , resulting in  $\bar{f}$  and a system of fluid equations that  $\bar{f}$  follows at the large scale. Conversely, Eq. (14) represents the transformation equation for the SPH operation between the macroscopic value  $\bar{f}$  and the microscopic value  $f$ ; in this case, the governing equations are the hydrodynamic equations that  $f$  follows on a large scale. However, in SPH computation, the physical quantity possessed by each particle is  $f$ , which is a small-scale quantity.  $\bar{f}$  is calculated on the large scale using the weight calculation on the right-hand side of Eq. (7) as a smoothing operation. However,  $\bar{f}$  always includes the fluctuation  $f_{\epsilon}^{\text{SPH}}$  caused by the smoothing kernel approximation error, as shown in Eq. (14). Consequently, the microscopic fluctuations  $f_{\epsilon}^{\text{SPH}}$  can be generated in the governing equations at the macroscopic scale. Here,  $f_{\epsilon}^{\text{SPH}}$  is proportional to the sum of the even powers of the smoothing width  $h$ , as shown on the right-hand side of Eq. (10). Therefore, as width  $h$  increases, so does  $f_{\epsilon}^{\text{SPH}}$ . Consequently,  $\bar{f}$  contains an amplified version of  $f_{\epsilon}^{\text{SPH}}$  compared with the original value, thus reproducing the microscopic behavior even at different large scales. Briefly, the SPH form serves as a magnifying glass for microscopic phenomena. Therefore, macroscopic quantum phenomena were replicated in our simulations, even by solving a system of equations on the hydrodynamic scale.

The SPH form has two errors: the smoothing kernel approximation and particle approximation errors. The smoothing kernel approximation error is inherent in the SPH form and exists as long as the width  $h$  is within the range of finite values. In short, this error is inherent in the approximation theory, which approximates the Dirac delta function with a finite-width distribution. By contrast, the particle approximation error is a discretization error that occurs when the kernel function is reproduced on a computer. If the regularity and  $h$ -connectivity conditions are satisfied, the discretization error can be minimized by increasing the resolution [82, 83]. Thus, the two error types exhibit different characteristics. We omitted the particle approximation error from the discussion here because it is a computational problem that can be minimized by ultra-high-resolution calculations on supercomputers if the appropriate discrete SPH forms are implemented; however, this is not an essential matter. Nevertheless, this argument can be extended to include truncation errors involving particle approximation. The relationship between kernel approximation errors, particle approximation errors, and true values in SPH is reported in Ref. [84]. Let  $f$  be the true value,  $f^s$  the kernel approximation value of  $f$ , and  $f^p$  the particle approximation value of  $f^s$ . Additionally, let  $f_{\epsilon}^s$  be the kernel approximation error,  $f_{\epsilon}^p$  the particle approximation error, and  $f_{\epsilon}$  the entire truncation error. We have the relationship  $f_{\epsilon} = (f^p - f) = (f^s - f) + (f^p - f^s) = (f_{\epsilon}^s + f_{\epsilon}^p)$ . Accordingly,  $f_{\epsilon}^{\text{SPH}}$  in Eq. (14) can be reinterpreted to include the particle approximation error. In this case,  $f_{\epsilon}^{\text{SPH}}$  does not necessarily correspond to  $-f_{\epsilon}^{\text{LES}}$  because it is established only when

kernel approximation errors are considered. In addition, numerical instability produces unpredictable errors in actual calculations [85, 86]. The equality between  $f_\epsilon^{\text{SPH}}$  and  $-f_\epsilon^{\text{LES}}$  is a formal relationship that holds when the particle approximation and numerical errors are ignored. In summary, we presented the equivalence between the spatial filtering of the LES and the kernel approximation of SPH; both are formally related as scale and inverse scale transformations in multiscale physics.

### 3.2. Subgrid-scale (SGS) model for the multi-scale cryogenic liquid helium-4

Suppose that  $\rho, \rho_s, \rho_n, \sigma,$  and  $\eta$  in Figs. 5(4) and (5) are constant parameters. By decomposing  $\mathbf{v}_s, \mathbf{v}_n, P, T,$  and  $\mathbf{F}_{sn}$  into the filtered and fluctuation components as  $\mathbf{v}_s = \bar{\mathbf{v}}_s + \mathbf{v}_\epsilon^{(s)}, \mathbf{v}_n = \bar{\mathbf{v}}_n + \mathbf{v}_\epsilon^{(n)}, P = \bar{P} + P_\epsilon, T = \bar{T} + T_\epsilon,$  and  $\mathbf{F}_{sn} = \bar{\mathbf{F}}_{sn} + \mathbf{F}_\epsilon,$  and by filtering Figs. 5(4) and (5) using Eq. (2), we obtain a system of equations for the two-fluid model at large scales, as follows:

$$\rho_s \frac{D\bar{\mathbf{v}}_s}{Dt} = -\frac{\rho_s}{\rho} \nabla \bar{P} + \rho_s \sigma \nabla \bar{T} - \bar{\mathbf{F}}_{sn}, \quad (15)$$

$$\rho_n \frac{D\bar{\mathbf{v}}_n}{Dt} = -\frac{\rho_n}{\rho} \nabla \bar{P} - \rho_s \sigma \nabla \bar{T} + \eta_n \nabla^2 \bar{\mathbf{v}}_n - \nabla \cdot \boldsymbol{\tau}_{SGS} + \bar{\mathbf{F}}_{sn}. \quad (16)$$

Here,  $\boldsymbol{\tau}_{SGS}$  is the SGS stress, whose components  $\tau_{SGS,ij}$  are given as

$$\tau_{SGS,ij} \equiv R_{ij} + L_{ij} + C_{ij}, \quad (17)$$

$$R_{ij} = \overline{u'_i u'_j}, \quad (18)$$

$$L_{ij} = \overline{\bar{u}_i \bar{u}_j} - \overline{u'_i u'_j}, \quad (19)$$

$$C_{ij} = \overline{u'_i \bar{u}_j} + \overline{u'_j \bar{u}_i}, \quad (20)$$

where  $\mathbf{v}_n = (u_1, u_2, u_3)^T$  and  $i, j = 1, 2, 3$ . As for temperature  $T$ , we did not solve the heat transport equation by defining the heat flux. Although it may be necessary to do so in the future, we did not consider solving the heat-transport equation at this stage. Therefore,  $T$  should be treated as a constant. However, in the SPH calculations, the temperature is obtained by a weighted calculation using the smoothed kernel function with respect to neighboring particles; thus, it varies around the average value depending on the density distribution. Therefore,  $T = \bar{T} + T_\epsilon$  is always true and  $T$  can be treated as a single-value function of  $\rho$ . Briefly, the treatment in the equation is the same as that for  $P$ . Accordingly, we allow a formal scale transformation of the temperature. In addition, we did not delve into the detailed expression of  $\bar{\mathbf{F}}_{sn}$ . Our current understanding of the mutual friction force  $\mathbf{F}_{sn}$  is discussed later.

Comparing Eq. (16) and Fig. 5(3), the extended terms of the Condiff viscosity model, i.e., the fourth and fifth terms on the right-hand side of Fig. 5(3), correspond to the divergence of the SGS stress tensor ( $-\nabla \cdot \boldsymbol{\tau}_{SGS}$ ). This formal correspondence between these parts of the viscosity model is reasonable in terms of multiscale physics. First, the extension of the viscosity term shown in Fig. 5(2) to that in Fig. 5(3) is to quantize the rotational angular momentum for each constituent particle to reproduce the nondissipative vortices. In particular, the fifth term on the right-hand side of Fig. 5(3) is designed to parameterize the internal degrees of freedom of the microscopic molecules. In other words, the fifth term on the right-hand side of Fig. 5(3) conveys the properties of the small vortices below the SGS (quantum vortices) in the classical system of hydrodynamics equations to the macro scale. Similarly, the divergence of the stress tensor at the SGS ( $-\nabla \cdot \boldsymbol{\tau}_{SGS}$ ) transfers the microscale eddy contributions to the larger scale, as discussed at the beginning of this section. Both viscosity models are consistent not only in form but also in physical meaning. Meanwhile, the SGS model assumes that the vortices dissipate below the Kolmogorov microscale; it would be natural to consider the cryogenic liquid helium-4 as an exceptional case where the vortices do not dissipate owing to the loss of viscosity even below the Kolmogorov microscale. We can also have the following assumption otherwise. Let us focus on the case of a high Reynolds number. Several experiments have revealed that the viscosity decreases by approximately 1/8 before and after the critical temperature [3, 5]. The Kolmogorov microscopic scale  $l$  is given by  $l = (\nu^3/\epsilon)^{1/4}$ , where  $\nu$  is the kinematic viscosity coefficient and  $\epsilon$  is the mean kinetic energy dissipation rate [67, 87, 88]. Thus, even if the viscosity is reduced by a factor of 8,  $l$  only becomes approximately  $4.7568 \dots \approx 4.8$  times smaller. Thus, the order of the Kolmogorov microscale remains the same. Generally, the Kolmogorov scale of liquid helium-4 is recognized on the scale of nanometers [89–91]. In contrast, the size of the velocity field created by a single quantum

vortex, as mentioned in the Introduction, is  $10^{-2}$  cm, or a few hundred micrometers, if estimated in terms of the lattice spacing of the quantum vortex lattice. Briefly, though the quantum vortex itself is on the angstrom scale, the velocity field it creates around it, i.e., the effective size of the quantum vortex, spans a few hundred micrometers. Therefore, the SGS model can be applied to quantum hydrodynamic problems if we focus on their effective sizes. The viscosity terms shown in Fig. 5(3) are a model dedicated to two-dimensional (2D) problems and cannot be directly applied to three-dimensional (3D) problems, except for a few quasi-two-dimensional cases. In this regard, the SGS model has a general form comprising 3D cases. Hence, if the properties of the quantum vortex, such as the interaction between the quantum vortex tubes, are accurately modeled in  $-\nabla \cdot \boldsymbol{\tau}_{SGS}$ , it is likely that the quantum mechanical effects will be transferred to the classical hydrodynamics equation system in the 3D problem.

Furthermore, we have the following perspective on  $\mathbf{F}_{sn}$  at the microscopic scale. According to quantum hydrodynamics, the mutual friction force  $\mathbf{F}_{sn}$  is proportional to the product of the instantaneous local relative velocity  $\mathbf{v}_{sn}$  and the square of the ensemble average of the relative velocity  $\mathbf{U}_{sn}$ , which is correlated with the statistical average of the vortex line density [18, 92]. This relationship is expressed as follows [93–96]:

$$\mathbf{F}_{sn} = A\rho_s\rho_n U_{sn}^2 \mathbf{v}_{sn} = \frac{2}{3}\rho_s\alpha\kappa L\mathbf{v}_{sn}, \quad (21)$$

where  $U_{sn} = \sqrt{|\mathbf{U}_{sn}|^2}$  and  $A$  is a constant parameter.  $\rho_s$  and  $\rho_n$  are the mass densities of the superfluid and normal fluid, respectively.  $\alpha$  denotes the mutual friction coefficient.  $\kappa$  is the quantum of the circulation.  $L$  is the vortex line density, which is obtained as the average length of the vortex configuration over the reduced volume  $\Omega$  as follows:

$$L = \frac{1}{\Omega} \int_{\Omega} d\xi, \quad (22)$$

where  $\xi$  represents the positions of the vortex lines in  $\Omega$ . Equation (21) shows that  $U_{sn}^2$  is represented as  $U_{sn}^2 = (\frac{2\alpha\kappa}{3A\rho_n})L$ , indicating that the substance of  $U_{sn}^2$  is the spatial average of the vortex line density  $L$ .

Accordingly, we can determine that  $U_{sn}^2$  is a macroscopic quantity in quantum hydrodynamics. If the average to obtain  $U_{sn}^2$  is sufficiently macroscopic to reach the hydrodynamic scale,  $U_{sn}^2$  can be reused in filtering, and only the fluctuation of the relative velocity  $\mathbf{v}_{sn}$  needs to be considered as  $\mathbf{F}_{sn} = A\rho_s\rho_n \overline{U_{sn}^2}(\mathbf{v}_{sn} + \mathbf{v}_\epsilon)$ . However, if the range of velocities for the average is still small compared to the hydrodynamic scale,  $U_{sn}^2$  must also account for the velocity fluctuations as  $\mathbf{F}_{sn} = A\rho_s\rho_n(|\mathbf{U}_{sn} + \mathbf{U}_\epsilon|)^2(\mathbf{v}_{sn} + \mathbf{v}_\epsilon)$ . In the latter case, the nonlinear effects manifest more readily. Future studies should examine the nonlinear effects of  $\overline{\mathbf{F}_{sn}}$ .

### 3.3. A proposed view on the composition of liquid helium at microscopic scales

In this paper, we have discussed the possibility that two-fluid models based on classical and quantum hydrodynamics have a relationship between the scale transformation by LES and the inverse scale transformation by SPH in liquid helium-4. We also pointed out that when we solved the two-fluid model based on classical hydrodynamics using SPH, the model errors in the smoothing kernel approximation error can substitute the variation at the microscopic scale and can be reproduced at more macroscopic scales according to the size of the kernel radius  $h$ . Let us now focus on the spatial occupancy of the inviscid or viscous component, or the superfluid or normal fluid component, and discuss the correspondence between these four concepts. Originally, the two-fluid model proposed by Landau was based on the concept that inviscid and viscous components coexist independently in an identical system. This concept has been modified accordingly. In the two-fluid model based on quantum hydrodynamics, only the normal fluid components, that is, the average flow of the excited quantum fluids, occupy the entire space; however, they are influenced by the entanglements of the quantum vortices, which are only sequences of singular points if viewed from the macroscopic scale. At present, normal fluids are generally accepted as a gathering of viscous fluid particles, but this concept may be incorrect because the viscous loss of the bulk liquid helium-4 in macroscopic quantum phenomena cannot coincide with the current picture of the two-fluid model based on quantum hydrodynamics, as the entire space is occupied only by viscous fluid particles. Accordingly, the correspondence between the four concepts of inviscid fluid, viscous fluid, superfluid, and normal fluid must be modified.

Figure 6 presents the proposed concept of the microscopic composition of the cryogenic liquid helium-4 in a multiscale framework. That is, at finite cryogenic temperatures, liquid helium-4 can be described as the average flow

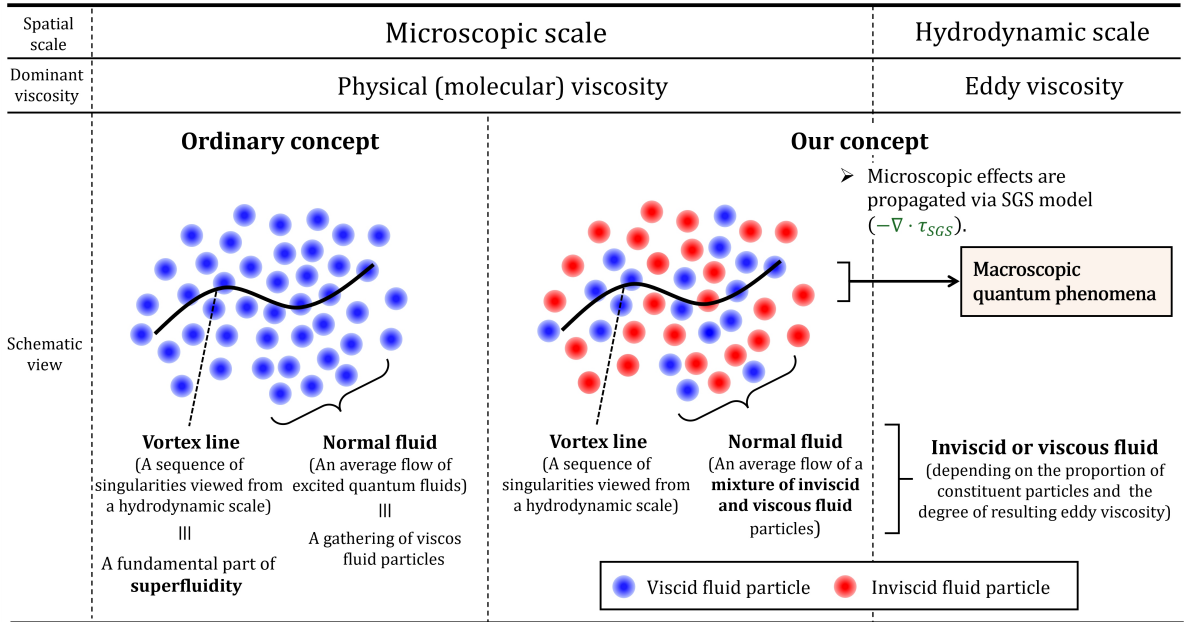


Figure 6: A proposed view of the microscopic composition of cryogenic liquid helium-4 in a multiscale framework.

of a mixture of inviscid and viscous fluid particles; because it contains viscous fluid particles, the fluid as a whole is considered a normal fluid. At this time, on the macroscopic scale, the fluid is classified as an inviscid fluid because the liquid viscosity due to the physical (molecular) viscosity is not yet sufficient to produce eddy viscosity on the hydrodynamic scale. As the temperature increases further, the ratio of viscous to inviscid fluid particles increases, and the eddy viscosity becomes sufficient for the fluid to be identified as viscous. The proposed concept clearly differs from the conventional view that normal fluids correspond exclusively to viscous fluids. However, our concept is more consistent with the original Landau two-fluid model because we allow for the existence of both inviscid and viscous fluid components. Recall that in the counterflow simulations shown in Fig. 3, the geometric correspondence between the distribution of the normal fluid and that of the vortex line density succeeded in replicating the tail-flattened profile. This enables us to postulate that, at finite temperatures, some of the remaining viscous fluid particles may serve as seeds for the quantum vortex lines because they have the potential to induce the ionization of fields. Impurities in helium-3 or ions in cryogenic liquid helium-4 are known to generate quantum vortex loops or rings [97–102], and this can qualitatively support the validity of simulations assuming that normal fluid components serve as vortex cores. This view should also be reasonable in terms of classical hydrodynamics, in that the vortex is a low-density area in the fluid, as normal fluid components can always be low-density components at cryogenic temperatures, as indicated by the BEC theory. In summary, the following conclusions can be drawn: First, a normal fluid can be a mixture of inviscid and viscous fluid particles. Second, a flow identified as a normal fluid on the microscopic scale because of the presence of molecular viscosity is still classified as an inviscid fluid on the hydrodynamic scale because its viscosity is not sufficient to produce vortex viscosity. Third, at finite temperatures, some of the remaining viscous fluid particles may serve as seeds for quantum vortex lines because they can induce field ionization.

#### 4. Conclusion

Our recent numerical studies on the cryogenic liquid helium-4 strongly indicate the features of multiscale physics that can be identified using the two-fluid model. In this paper, we have presented that two-fluid models based on classical and quantum hydrodynamics have a relationship between the scale transformation by LES and the inverse scale transformation by SPH in liquid helium-4. We showed that the spin angle momentum conservation term, which we previously introduced into the two-fluid model as a quantum mechanical correction, formally corresponds to the SGS model, which can be derived from the scale transformation of the two-fluid model from quantum to classical hydrodynamics. We also showed that solving the two-fluid model based on classical hydrodynamics using SPH can reproduce the fluctuations at the microscopic scale because the truncation errors owing to the smoothing kernel

approximation can substitute the fluctuations at the microscopic scale. In particular, the fluctuations can be reproduced at more macroscopic scales and amplified according to the size of the kernel radius. Our results and discussion provide new insights into the microscopic composition of cryogenic liquid helium-4 within a multiscale framework. First, a normal fluid can be a mixture of inviscid and viscous particles. Second, a flow identified as a normal fluid on the microscopic scale because of the presence of molecular viscosity is still classified as an inviscid fluid on the hydrodynamic scale because its viscosity is insufficient to produce eddy viscosity. In conclusion, we have provided a new multiscale physical framework for cryogenic liquid helium-4.

## Acknowledgment

This study was supported by JSPS KAKENHI Grant Number 22K14177 and JST PRESTO, Grant Number JP-MJPR2307. The authors thank Editage ([www.editage.jp](http://www.editage.jp)) for the English language editing. The author would also like to express gratitude to his family for their moral support and encouragement.

## References

- [1] H. K. Onnes, Part i. laboratory methods of liquefaction. on the lowest temperature yet obtained, *Trans. Faraday Soc.* **18**, 145 (1922).
- [2] H. K. Onnes, *“The liquefaction of helium.”* (Springer Netherlands, Dordrecht, 1991), pp. 164–187.
- [3] P. Kapitza, Viscosity of liquid helium below the  $\lambda$ -point, *Nature* **141**, 74 (1938).
- [4] F. LONDON, The  $\lambda$ -phenomenon of liquid helium and the bose-einstein degeneracy, *Nature* **141**, 643 (1938).
- [5] E. F. BURTON, Viscosity of helium i and helium ii, *Nature* **135**, 265 (1935).
- [6] J. F. ALLEN and A. D. MISENER, Flow of liquid helium ii, *Nature* **141**, 75 (1938).
- [7] K. Atkins, Wave propagation and flow in liquid helium ii, *Advances in Physics* **1**, 169 (1952).
- [8] R. Dingle, Theories of helium ii, *Advances in Physics* **1**, 111 (1952).
- [9] L. TISZA, Transport phenomena in helium ii, *Nature* **141**, 913 (1938).
- [10] L. Landau, Theory of the superfluidity of helium ii, *Phys. Rev.* **60**, 356 (1941).
- [11] C. Gorter and J. Mellink, On the irreversible processes in liquid helium ii, *Physica* **15**, 285 (1949).
- [12] R. Feynman, Chapter ii application of quantum mechanics to liquid helium, volume 1 of *Progress in Low Temperature Physics*, pp. 17–53, Elsevier, 1955.
- [13] K. W. Schwarz, Three-dimensional vortex dynamics in superfluid  $^4\text{He}$ : Line-line and line-boundary interactions, *Phys. Rev. B* **31**, 5782 (1985).
- [14] K. W. Schwarz, Three-dimensional vortex dynamics in superfluid  $^4\text{He}$ : Homogeneous superfluid turbulence, *Phys. Rev. B* **38**, 2398 (1988).
- [15] M. Tsubota and M. Kobayashi, Chapter 1 - energy spectra of quantum turbulence, in *Quantum Turbulence*, edited by M. Tsubota and W. Halperin, volume 16 of *Progress in Low Temperature Physics*, pp. 1–43, Elsevier, 2009.
- [16] R. Hänninen and A. W. Baggaley, Vortex filament method as a tool for computational visualization of quantum turbulence, *Proceedings of the National Academy of Sciences* **111**, 4667 (2014).
- [17] O. C. Idowu, D. Kivotides, C. F. Barenghi, and D. C. Samuels, *Numerical Methods for Coupled Normal-Fluid and Superfluid Flows in Helium II* (Springer Berlin Heidelberg, Berlin, Heidelberg, 2001), pp. 162–176.
- [18] A. W. Baggaley and S. Laizet, Vortex line density in counterflowing he ii with laminar and turbulent normal fluid velocity profiles, *Physics of Fluids* **25**, 115101 (2013).
- [19] S. Yui, M. Tsubota, and H. Kobayashi, Three-dimensional coupled dynamics of the two-fluid model in superfluid  $^4\text{He}$ : Deformed velocity profile of normal fluid in thermal counterflow, *Phys. Rev. Lett.* **120**, 155301 (2018).
- [20] C. L. Horner and R. A. Van Gorder, Dynamics of quantized vortex filaments under a local induction approximation with second-order correction, *Physics of Fluids* **31**, 065103 (2019), <https://doi.org/10.1063/1.5091567>.
- [21] S. Yui, H. Kobayashi, M. Tsubota, and W. Guo, Fully coupled two-fluid dynamics in superfluid  $^4\text{He}$ : Anomalous anisotropic velocity fluctuations in counterflow, *Phys. Rev. Lett.* **124**, 155301 (2020).
- [22] H. Kojima, W. Veith, E. Guyon, and I. Rudnick, Persistent current states in rotating superfluid helium, *Journal of Low Temperature Physics* **8**, 187 (1972).
- [23] E. J. Yarmchuk and R. E. Packard, Photographic studies of quantized vortex lines, *Journal of Low Temperature Physics* **46**, 479 (1982).
- [24] K. W. Madison, F. Chevy, V. Bretin, and J. Dalibard, Stationary states of a rotating bose-einstein condensate: Routes to vortex nucleation, *Phys. Rev. Lett.* **86**, 4443 (2001).
- [25] M. Tsubota, K. Kasamatsu, and M. Ueda, Vortex lattice formation in a rotating bose-einstein condensate, *Phys. Rev. A* **65**, 023603 (2002).
- [26] K. Kasamatsu, M. Tsubota, and M. Ueda, Nonlinear dynamics of vortex lattice formation in a rotating bose-einstein condensate, *Phys. Rev. A* **67**, 033610 (2003).
- [27] S. K. Adhikari, Vortex-lattice formation in a spin-orbit coupled rotating spin-1 condensate, *Journal of Physics: Condensed Matter* **33**, 065404 (2020).
- [28] S. Tsuzuki, Reproduction of vortex lattices in the simulations of rotating liquid helium-4 by numerically solving the two-fluid model using smoothed-particle hydrodynamics incorporating vortex dynamics, *Physics of Fluids* **33**, 087117 (2021), <https://doi.org/10.1063/5.0060605>.
- [29] S. Tsuzuki, Numerical model of the gross-pitaevskii equation for rotating bose-einstein condensates using smoothed-particle hydrodynamics, *Physics of Fluids* **35**, 047102 (2023).

- [30] S. Tsuzuki, E. Itoh, and K. Nishinari, Three-dimensional analysis of vortex-lattice formation in rotating bose–einstein condensates using smoothed-particle hydrodynamics, *Journal of Physics Communications* **7**, 121001 (2023).
- [31] W. F. Vinen, *The physics of superfluid helium*, (2004).
- [32] M. L. Amigo *et al.*, A quantitative experiment on the fountain effect in superfluid helium, *European Journal of Physics* **38**, 055103 (2017).
- [33] R. Feynman, *Progress in low temperature physics*, (1955).
- [34] S. W. Van Sciver and C. F. Barenghi, Chapter 5 - visualisation of quantum turbulence, in *Quantum Turbulence*, edited by M. Tsubota and W. Halperin, volume 16 of *Progress in Low Temperature Physics*, pp. 247–303, Elsevier, 2009.
- [35] A. C. Hollis-Hallett, Experiments with a rotating cylinder viscometer in liquid helium ii, *Mathematical Proceedings of the Cambridge Philosophical Society* **49**, 717–727 (1953).
- [36] S. Tsuzuki, Theoretical framework bridging classical and quantum mechanics for the dynamics of cryogenic liquid helium-4 using smoothed-particle hydrodynamics, *Physics of Fluids* **34**, 127116 (2022), <https://doi.org/10.1063/5.0122247>.
- [37] S. Tsuzuki, A hydrodynamic approach to reproduce multiple spinning vortices in horizontally rotating three-dimensional liquid helium-4, *Physics of Fluids* **36**, 087155 (2024).
- [38] R. A. Gingold and J. J. Monaghan, Smoothed particle hydrodynamics: theory and application to non-spherical stars, *Monthly notices of the royal astronomical society* **181**, 375 (1977).
- [39] J. Monaghan and J. Lattanzio, A refined particle method for astrophysical problems, *Astronomy and Astrophysics* **149**, 135 (1985).
- [40] J. J. Monaghan, Smoothed particle hydrodynamics, *Annual review of astronomy and astrophysics* **30**, 543 (1992).
- [41] J. Monaghan, Simulating free surface flows with sph, *Journal of Computational Physics* **110**, 399 (1994).
- [42] J. Monaghan and A. Kocharyan, Sph simulation of multi-phase flow, *Computer Physics Communications* **87**, 225 (1995), *Particle Simulation Methods*.
- [43] J. Morris and J. Monaghan, A switch to reduce sph viscosity, *Journal of Computational Physics* **136**, 41 (1997).
- [44] J. J. Monaghan, Smoothed particle hydrodynamics, *Reports on Progress in Physics* **68**, 1703 (2005).
- [45] D. W. Condiff and J. S. Dahler, Fluid mechanical aspects of antisymmetric stress, *The Physics of Fluids* **7**, 842 (1964).
- [46] K. Müller, D. A. Fedosov, and G. Gompper, Smoothed dissipative particle dynamics with angular momentum conservation, *Journal of Computational Physics* **281**, 301 (2015).
- [47] S. Tsuzuki, Particle approximation of the two-fluid model for superfluid 4he using smoothed particle hydrodynamics, *Journal of Physics Communications* **5**, 035001 (2021).
- [48] H. Kobayashi, S. Yui, and M. Tsubota, Numerical study on entrance length in thermal counterflow of superfluid 4he, *Journal of Low Temperature Physics* **196**, 35 (2019).
- [49] A. Marakov *et al.*, Visualization of the normal-fluid turbulence in counterflowing superfluid <sup>4</sup>He, *Phys. Rev. B* **91**, 094503 (2015).
- [50] X. Xu and X.-L. Deng, An improved weakly compressible sph method for simulating free surface flows of viscous and viscoelastic fluids, *Computer Physics Communications* **201**, 43 (2016).
- [51] W. C. Schieve and L. P. Horwitz, *Bose–Einstein ideal gas condensation* (Cambridge University Press, 2009), pp. 141–158.
- [52] J. M. Ziman and M. H. L. Pryce, Quantum hydrodynamics and the theory of liquid helium, *Proceedings of the Royal Society of London. Series A. Mathematical and Physical Sciences* **219**, 257 (1953).
- [53] *Second Quantization* (Springer Netherlands, Dordrecht, 2009), pp. 109–128.
- [54] M. Schönberg, A general theory of the second quantization methods, *Il Nuovo Cimento (1943-1954)* **10**, 697 (1953).
- [55] D. P. Sankovich, Bogolyubov’s theory of superfluidity, *Physics of Particles and Nuclei* **41**, 1068 (2010).
- [56] E. P. Gross, Structure of a quantized vortex in boson systems, *Il Nuovo Cimento (1955-1965)* **20**, 454 (1961).
- [57] L. P. Pitaevskii, Vortex lines in an imperfect bose gas, *Sov. Phys. JETP* **13**, 451 (1961).
- [58] I. M. Khalatnikov, *An introduction to the theory of superfluidity* (CRC Press, 2018).
- [59] V. F. Sears, E. C. Svensson, P. Martel, and A. D. B. Woods, Neutron-scattering determination of the momentum distribution and the condensate fraction in liquid <sup>4</sup>He, *Phys. Rev. Lett.* **49**, 279 (1982).
- [60] M. Robinson, M. Ramaioli, and S. Luding, Fluid-article flow simulations using two-way-coupled mesoscale sph-dem and validation, *International Journal of Multiphase Flow* **59**, 121 (2014).
- [61] Y. He *et al.*, A gpu-based coupled sph-dem method for particle-fluid flow with free surfaces, *Powder Technology* **338**, 548 (2018).
- [62] J. Pozorski and M. Olejnik, Smoothed particle hydrodynamics modelling of multiphase flows: an overview, *Acta Mechanica* **235**, 1685 (2024).
- [63] J. C. Maxwell, V. illustrations of the dynamical theory of gases.–part i. on the motions and collisions of perfectly elastic spheres, *The London, Edinburgh, and Dublin Philosophical Magazine and Journal of Science* **19**, 19 (1860).
- [64] S. G. Brush, Theories of liquid viscosity., *Chemical Reviews* **62**, 513 (1962).
- [65] J. C. Maxwell, *Maxwell on molecules and gases* (Mit Press, 1986).
- [66] N. D. Katopodes, Chapter 8 - turbulent flow, in *Free-Surface Flow*, edited by N. D. Katopodes, pp. 566–650, Butterworth-Heinemann, 2019.
- [67] A. M. Steinberg, P. E. Hamlington, and X. Zhao, Structure and dynamics of highly turbulent premixed combustion, *Progress in Energy and Combustion Science* **85**, 100900 (2021).
- [68] R. J. Doviak and D. S. Zrnić, 11 - observations of fair weather, in *Doppler Radar and Weather Observations (Second Edition)*, edited by R. J. Doviak and D. S. Zrnić, pp. 424–505, Academic Press, San Diego, , second edition ed., 1993.
- [69] A. N. Kolmogorov, The local structure of turbulence in incompressible viscous fluid for very large reynolds, Numbers. In *Dokl. Akad. Nauk SSSR* **30**, 301 (1941).
- [70] A. Obhukov, Energy distribution in the spectrum of turbulent flow, *Izv. Akad. Nauk SSSR, Ser. Geofiz* **5**, 453 (1941).
- [71] J. M. McDonough, Introductory lectures on turbulence: physics, mathematics and modeling, (2007).
- [72] J. W. Deardorff, A numerical study of three-dimensional turbulent channel flow at large reynolds numbers, *Journal of Fluid Mechanics* **41**, 453–480 (1970).
- [73] A. Leonard, Energy cascade in large-eddy simulations of turbulent fluid flows, in *Turbulent Diffusion in Environmental Pollution*, edited by

- F. Frenkiel and R. Munn, volume 18 of *Advances in Geophysics*, pp. 237–248, Elsevier, 1975.
- [74] R. Kara, Fundamentals and theory of large eddy simulation, in *Computational Fluid Dynamics - Analysis, Simulations, and Applications*, edited by P. M. Baccouch, chap. 0, IntechOpen, Rijeka, 2024.
- [75] O. Reynolds, Iv. on the dynamical theory of incompressible viscous fluids and the determination of the criterion, *Philosophical Transactions of the Royal Society of London. (A.)* **186**, 123 (1895).
- [76] M. Desbrun and M.-P. Gascuel, Smoothed particles: A new paradigm for animating highly deformable bodies, in *Computer Animation and Simulation '96*, pp. 61–76, Springer, 1996.
- [77] M. Müller, D. Charypar, and M. Gross, Particle-based fluid simulation for interactive applications, in *Proceedings of the Eurographics symposium on Computer animation*, pp. 154–159, Eurographics Association, 2003.
- [78] T. Stranex and S. Wheaton, A new corrective scheme for sph, *Computer Methods in Applied Mechanics and Engineering* **200**, 392 (2011).
- [79] R. Gabbasov, L. D. G. Sigalotti, F. Cruz, J. Klapp, and J. M. Ramírez-Velasquez, Consistent sph simulations of protostellar collapse and fragmentation, *The Astrophysical Journal* **835**, 287 (2017).
- [80] L. D. G. Sigalotti, O. Rendón, J. Klapp, C. A. Vargas, and F. Cruz, A new insight into the consistency of the sph interpolation formula, *Applied Mathematics and Computation* **356**, 50 (2019).
- [81] A. Di Mascio, M. Antuono, A. Colagrossi, and S. Marrone, Smoothed particle hydrodynamics method from a large eddy simulation perspective, *Physics of Fluids* **29**, 035102 (2017).
- [82] Y. Imoto, Unique solvability and stability analysis for incompressible smoothed particle hydrodynamics method, *Computational Particle Mechanics* **6**, 297 (2019).
- [83] Y. Imoto, Truncation error estimates of approximate operators in a generalized particle method, *Japan Journal of Industrial and Applied Mathematics* **37**, 565 (2020).
- [84] A. Amicarelli, J.-C. Marongiu, F. Leboeuf, J. Leduc, and J. Caro, Sph truncation error in estimating a 3d function, *Computers & Fluids* **44**, 279 (2011).
- [85] D. S. Balsara, von neumann stability analysis of smoothed particle hydrodynamics—suggestions for optimal algorithms, *Journal of Computational Physics* **121**, 357 (1995).
- [86] J. Swegle, D. Hicks, and S. Attaway, Smoothed particle hydrodynamics stability analysis, *Journal of Computational Physics* **116**, 123 (1995).
- [87] J. Gregory, Chapter 3 - floc formation and floc structure, in *Interface Science in Drinking Water Treatment*, edited by G. Newcombe and D. Dixon, volume 10 of *Interface Science and Technology*, pp. 25–43, Elsevier, 2006.
- [88] T. Okawa *et al.*, 3 - fundamentals for power engineering, in *Fundamentals of Thermal and Nuclear Power Generation*, edited by Y. Koizumi, T. Okawa, and S. Mori, volume 1 of *JSME Series in Thermal and Nuclear Power Generation*, pp. 77–226, Elsevier, 2021.
- [89] W. Guo, M. L. Mantia, D. P. Lathrop, and S. W. V. Sciver, Visualization of two-fluid flows of superfluid helium-4, *Proceedings of the National Academy of Sciences* **111**, 4653 (2014).
- [90] C. F. Barenghi, Y. A. Sergeev, and A. W. Baggaley, Regimes of turbulence without an energy cascade, *Scientific Reports* **6**, 35701 (2016).
- [91] L. Skrbek, D. Schmoranzler, Šimon Midlik, and K. R. Sreenivasan, Phenomenology of quantum turbulence in superfluid helium, *Proceedings of the National Academy of Sciences* **118**, e2018406118 (2021).
- [92] R. G. Cooper, M. Mesgarnizhad, A. W. Baggaley, and C. F. Barenghi, Knot spectrum of turbulence, *Scientific Reports* **9**, 10545 (2019).
- [93] W. F. Vinen and D. Shoenberg, Mutual friction in a heat current in liquid helium ii i. experiments on steady heat currents, *Proceedings of the Royal Society of London. Series A. Mathematical and Physical Sciences* **240**, 114 (1957).
- [94] W. F. Vinen and D. Shoenberg, Mutual friction in a heat current in liquid helium ii. ii. experiments on transient effects, *Proceedings of the Royal Society of London. Series A. Mathematical and Physical Sciences* **240**, 128 (1957).
- [95] W. F. Vinen and D. Shoenberg, Mutual friction in a heat current in liquid helium ii iii. theory of the mutual friction, *Proceedings of the Royal Society of London. Series A. Mathematical and Physical Sciences* **242**, 493 (1957).
- [96] W. F. Vinen and D. Shoenberg, Mutual friction in a heat current in liquid helium. ii. iv. critical heat currents in wide channels, *Proceedings of the Royal Society of London. Series A. Mathematical and Physical Sciences* **243**, 400 (1958).
- [97] G. W. Rayfield and F. Reif, Quantized vortex rings in superfluid helium, *Phys. Rev.* **136**, A1194 (1964).
- [98] C. M. Muirhead, W. F. Vinen, and R. J. Donnelly, The nucleation of vorticity by ions in superfluid  ${}^4\text{He}$  ii. theory of the effect of dissolved  ${}^3\text{He}$ , *Proceedings of the Royal Society of London. A. Mathematical and Physical Sciences* **402**, 225 (1985).
- [99] C. M. Muirhead *et al.*, The nucleation of vorticity by ions in superfluid  ${}^4\text{He}$  i. basic theory, *Philosophical Transactions of the Royal Society of London. Series A, Mathematical and Physical Sciences* **311**, 433 (1984).
- [100] P. C. Hendry, N. S. Lawson, P. V. E. McClintock, C. D. H. Williams, and R. M. Bowley, The breakdown of superfluidity in liquid  ${}^4\text{He}$  vi. macroscopic quantum tunnelling by vortices in isotopically pure  ${}^4\text{He}$  ii, *Philosophical Transactions of the Royal Society of London. Series A: Physical and Engineering Sciences* **332**, 387 (1990).
- [101] G. G. Nancolas, R. M. Bowley, P. V. E. McClintock, and W. F. Vinen, The breakdown of superfluidity in liquid  ${}^4\text{He}$ . iv. influence of  ${}^3\text{He}$  isotopic impurities on the nucleation of quantized vortex rings, *Philosophical Transactions of the Royal Society of London. Series A, Mathematical and Physical Sciences* **313**, 537 (1985).
- [102] R. M. Bowley and F. W. Sheard, Motion of negative ions at supercritical drift velocities in liquid  ${}^4\text{He}$  at low temperatures, *Phys. Rev. B* **16**, 244 (1977).